

Deep Interactive Segmentation of Medical Images: A Systematic Review and Taxonomy

Zdravko Marinov*, Paul F. Jäger*, Jan Egger, Jens Kleesiek, Rainer Stiefelhagen

Abstract—Interactive segmentation is a crucial research area in medical image analysis aiming to boost the efficiency of costly annotations by incorporating human feedback. This feedback takes the form of clicks, scribbles, or masks and allows for iterative refinement of the model output so as to efficiently guide the system towards the desired behavior. In recent years, deep learning-based approaches have propelled results to a new level causing a rapid growth in the field with 121 methods proposed in the medical imaging domain alone. In this review, we provide a structured overview of this emerging field featuring a comprehensive taxonomy, a systematic review of existing methods, and an in-depth analysis of current practices. Based on these contributions, we discuss the challenges and opportunities in the field. For instance, we find that there is a severe lack of comparison across methods which needs to be tackled by standardized baselines and benchmarks.

Index Terms—Deep learning, interactive segmentation, medical imaging, systematic review.

I. INTRODUCTION

DEEP LEARNING segmentation methods revolutionized various application areas including autonomous driving [158], product manufacturing [159], and medical image analysis [160]. For the latter, high-quality segmentation of anatomical structures and detection of abnormalities is an essential step towards automating diagnosis and treatment planning [161]. However, the quality of these methods relies heavily on large-scale data sets for training featuring high-quality annotations. Especially in the medical imaging domain, this poses a major bottleneck, because annotations are time-consuming and require expert knowledge [5]. For instance, labeling a volumetric Positron Emission Tomography/Computed Tomography (PET/CT) volume to identify tumor lesions can consume up to an hour of manual annotation for a single sample [154].

This work has been submitted to the IEEE for possible publication. Copyright may be transferred without notice, after which this version may no longer be accessible.

The present contribution is supported by the Helmholtz Association under the joint research school “HIDSS4Health – Helmholtz Information and Data Science School for Health.” (*Zdravko Marinov and *Paul F. Jäger are co-first authors.) (Corresponding author: Zdravko Marinov.)

Zdravko Marinov and Rainer Stiefelhagen are with the Computer Vision for Human-Computer Interaction Lab, Department of Informatics, Karlsruhe Institute of Technology, Adenauerring 10, 76131 Karlsruhe, Germany (e-mail: zdravko.marinov@kit.edu).

Jan Egger and Jens Kleesiek are with the Institute for Artificial Intelligence in Medicine (IKIM), University Hospital Essen (AöR), Girardetstraße 2, 45131 Essen, Germany.

Paul F. Jäger is with the German Cancer Research Center (DKFZ) Heidelberg, Interactive Machine Learning Group, Im Neuenheimer Feld 223, 69120 Heidelberg, Germany, and with the Helmholtz Imaging, DKFZ, Im Neuenheimer Feld 223, 69120 Heidelberg, Germany.

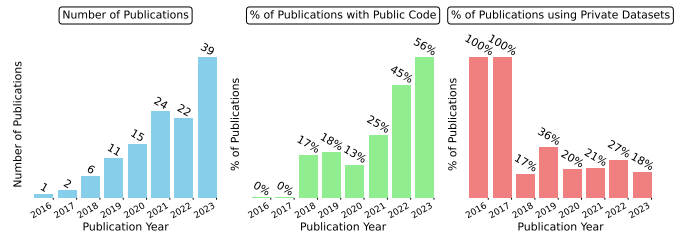


Fig. 1. Tendencies in medical interactive segmentation in recent years.

Deep interactive segmentation addresses this trade-off between high-quality segmentation and laborious manual annotation. The idea is to boost annotation efficiency by incorporating human feedback into either the training or application process of segmentation methods. This feedback loop lets users iteratively correct or refine the model output, e.g. in the form of clicks, scribbles, or fine-grained voxel-masks, and thus efficiently guide the model towards the desired output.

The field of interactive segmentation traces back to active contour models [153] and Graph Cut [131], which primarily rely on low-level image features, such as pixel intensity changes, to differentiate foreground and background. However, these traditional methods face challenges when dealing with ambiguous boundaries and do not incorporate high-level semantics related to the object-of-interest [5], [65], [140]. These challenges have been widely solved in recent years by interactive deep learning-based approaches, as first introduced by Xu et al. [140]. This paradigm shift has led to the successful application of interactive segmentation systems, for instance by reducing the annotation time of the aforementioned PET/CT volume to around three minutes [82].

Several reviews have been published in the field of interactive segmentation. However, previous reviews either focus on classical approaches rather than the more recent deep learning methods [145], [155], [156], [180], or exclude approaches from the medical domain [157]. At the same time, no review exists for the field of deep learning-based interactive segmentation of medical images despite its rapid emergence with over 121 proposed methods in the last 8 years as seen in Fig. 1. The lack of a systematic overview in this field hampers scientific progress by generating redundancies and poses a challenge for users seeking the best-fitting method for their problem.

We address these shortcomings in this dedicated review by means of the following key contributions:

- We introduce a comprehensive taxonomy for deep interactive segmentation allowing users to quickly comprehend the various approaches and select the best fitting

method for their task.

- Based on this taxonomy, we provide a systematic review of 121 proposed methods in the medical domain.
- We perform an in-depth analysis of the current practices in the field including prevalent datasets, anatomies, and validation metrics, as well as the adequacy of baselines and the reproducibility of results.
- Based on this analysis, we provide a discussion of current challenges and opportunities in the field.

II. TERMINOLOGY

Before we present our systematic review, we establish clear definitions for the fundamental terminology within the domain of interactive segmentation.

A. Interactive Segmentation

Interactive segmentation describes an iterative feedback loop, where user-provided corrections or refinements to the model’s output inform subsequent iterations, leading to updated predictions. Depending on the method, user guidance is provided during training or application in the form of, e.g., clicks, scribbles, or other interactions. Importantly, initial labels provided to a model before training are excluded from this definition to differentiate interactive segmentation from related training paradigms such as weakly-supervised segmentation.

B. Guidance Signal

A guidance signal is a representation of the user interactions in a form in which the model can process it. This can be an explicit representation that involves transforming the user interaction into an additional structured input for the model to process and learn from, e.g., Gaussian heatmaps centered around user clicks. Additionally, guidance signals can also be implicit, where user interaction information is subtly integrated into the model’s learning process without the provision of explicit structured input. For instance, this integration could involve modifying the loss function to incorporate the distance to clicks and assign greater weight to predictions in proximity to those clicks. Existing guidance signals for clicks, scribbles, and other interactions are given in the Appendixes.

C. Training and Application

We use the terms *training* and *application* as the building blocks of our taxonomy tree. In the training stage, the model undergoes optimization, where its weights are updated using a predetermined loss function. The subsequent application stage involves deploying the trained model on unseen data, utilizing its refined parameters to address specific clinical tasks.

D. Robot User

The concept of a robot user [122] involves creating a simulated model that mimics the behavior of a real human annotator. The robot user leverages ground-truth labels to simulate user interactions at plausible locations. For example, clicks can be sampled randomly from the ground-truth labels

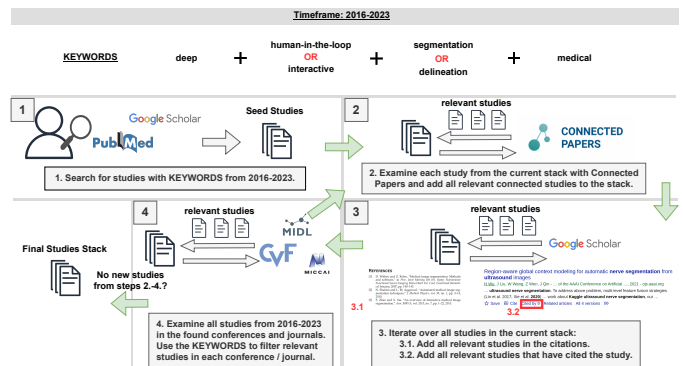


Fig. 2. Search strategy in our systematic review for selecting relevant studies. The logos in steps 1 and 4 are illustrated only as examples for literature databases and venues respectively. A full list is given in the Appendixes.

or generated at the center of the largest object. These simulated interactions are then converted into a guidance signal, which is fed back to the model. Robot users are used during training to simulate interactions for a large number of training samples as this is unfeasible for real human annotators at this scale. Additionally, robot users can also be used during application to evaluate trained models on unseen data without involving real human annotators. Robot users can be categorized as non-iterative or iterative. Non-iterative users simulate all interactions simultaneously, integrate them into the model, and perform a single prediction. In contrast, iterative users simulate interactions in a loop. In this case, the model predicts, interactions are generated based on the errors of this prediction, and the model predicts again using all the previous interactions in an interaction-prediction loop [152]. Here, an iteration denotes a single round of interaction and prediction with the model.

III. SCOPE AND STUDY COLLECTION STRATEGY

We conduct a systematic review of deep learning-based interactive segmentation models applied in medical scenarios. Our review, being inherently technical in nature, aims to rigorously categorize and analyze relevant literature. Recognizing the need for a comprehensive reporting framework, we integrate as many components from the Preferred Reporting Items for Systematic Reviews and Meta-Analyses (PRISMA) guidelines by Moher et al. [139] as applicable to enhance the transparency and methodological clarity of our study. A detailed account of the adopted PRISMA components can be found in the PRISMA 2020 checklist in the Appendixes. We performed a literature search in several databases, including PubMed, Google Scholar, IEEE Xplore, SpringerLink, and arXiv, using specific keywords – [interactive], [human-in-the-loop], [segmentation], [delineation], [medical], and [deep]. The search was carried out on 31 July 2023, and we limited the publication period to cover the years 2016–2023 since the first deep learning interactive method originated in 2016 [140]. We removed duplicates, including pre-prints followed by their peer-reviewed versions. Subsequently, we conducted an initial manual screening of titles and abstracts to ensure that the selected studies are relevant. After this initial screening, full texts were retrieved and reviewed for eligibility based on

specific inclusion criteria: 1) studies with English full texts; 2) studies that have undergone peer-review or have pre-prints submitted to the arXiv database; and 3) studies describing the application of interactive segmentation models for a human medical purpose. Consequently, certain exclusion criteria were applied to maintain the focus and quality of the review: 1) studies lacking English full texts; 2) studies that utilize non-deep learning models; 3) studies that utilize interactive models solely on natural images; and 4) studies using medical images but not as the primary focus.

One reviewer assessed a study’s eligibility through a three-stage process. Initially, we examine the title to decide if it focuses on deep medical interactive segmentation. If the title is ambiguous, we read the abstract for confirmation. In cases where the abstract remains unclear, we read the entire study.

This search produced our initial *seed studies* stack as illustrated in Fig. 2. In addition to adhering to the PRISMA guidelines, we implemented three supplementary steps in our search strategy to maximize the retrieval of relevant studies and formed an iterative loop utilizing these steps. These steps are depicted as steps 2, 3, and 4 in Fig. 2. In step 2, we incorporated the Connected Papers tool¹ to enhance our search process. This tool was applied to each of the already included studies from the *seed studies*, and we systematically screened all the suggested studies recommended by the tool, ensuring they meet our predefined inclusion and exclusion criteria. In step 3, we manually inspected all the citations of each study in the *seed studies* and all of the studies that have cited this study using the “Cited by” function in Google Scholar. In step 4, we formed a list of all the peer-reviewed venues, which is given in the Appendixes, and manually screened all of the publications from each venue in the timeframe 2016–2023 with our predefined keywords and added the relevant publications in our *seed studies*. We repeated steps 2, 3, and 4 and accumulated all relevant studies in our *seed studies* stack until no new relevant studies were found. Our search strategy found a total of 121 relevant publications.

After collecting all studies, one reviewer manually extracted from each study the following data items: 1) used imaging modalities; 2) used datasets along with provided links, if available; 3) prior interactive methods the study has compared to; 4) employed evaluation metrics; 5) type of interaction, e.g., clicks; 6) target structures for segmentation; 7) and, if applicable, a link to publicly available code. We cataloged all 121 reviewed studies and their data items in Tables I and II. This facilitates efficient navigation for future researchers seeking relevant interactive methods related to their own work.

It is important to note that during our search we exclude “classical approaches”, which do not utilize deep learning. Some examples include methods based on: 1) Graph Cut [131], [141]; 2) dense Conditional Random Fields (CRFs) [166]; 3) active contours [153]; and 4) level sets [167]. While non-deep learning interactive frameworks such as ilastik [168] and ITK-Snap [169] have demonstrated success in clinical workflows, we maintain a focus on deep learning-based methods to

align with the review’s scope and the growing prevalence of interactive deep learning models in the medical domain.

IV. TAXONOMY

After retrieving the 121 publications, we analyze the foundational principles of their methodologies and categorize them based on common characteristics. This procedure yields our proposed *taxonomy tree* and *taxonomy blueprints* in Fig. 3 and 4, which function as navigational tools for existing medical interactive segmentation methods. These tools should help researchers categorize their approaches and steer them towards existing methods that align with their own. In this section, we provide detailed insights into the construction of both tools.

Taxonomy tree. In our systematic review of deep medical interactive segmentation, we identified three paradigms that are determined by the stage at which human interactions occur. These paradigms form the primary categorization in our taxonomy tree in Fig. 3, and a summary of each paradigm can be found in the three boxes at the bottom right. The interactions take place in two distinct stages: training and application, which are defined in Section II-C. Depending on these two stages, interactions can occur: 1) exclusively during application; 2) exclusively during training; 3) or in an alternating manner between both stages (online learning). These three paradigms constitute our proposed taxonomy and are described in detail in Sections IV-B, IV-A, and IV-C.

Taxonomy blueprints. Fig. 4 visually depicts the training and application phases of the main taxonomy nodes, using icons to represent generic concepts, such as the input image. The diagram displays the involvement of a human annotator during either the training or application phase. The distinction between training and application phases is apparent in most paradigms, however, in the case of the *online learning* paradigm, this separation is not as evident. In *online learning*, the model is alternately trained and applied to the same data, with real-time feedback provided by a human annotator. The taxonomy blueprints offer a two-fold advantage: 1) they reveal detailed differences in training and application phases among nodes in the taxonomy tree; 2) and streamline the categorization of emerging methods. They serve as a visual guide to both understand the taxonomy nodes and systematically incorporate new approaches into the existing taxonomy structure.

A. Training Only

The first taxonomy category encompasses methods that utilize human interactions only during training and is highlighted as yellow nodes in the taxonomy tree in Fig. 3. In this paradigm, also referred to as “Active Learning”, models are first trained on a small labeled fraction of the dataset (“starting budget”) and are subsequently applied to the unlabeled remainder of the dataset. Based on these predictions, the most informative samples for future training are identified, annotated, and added to the training data for the next iteration. This iterative training process continues until the annotator is content with the model’s predictions. Afterward, the model can be used non-interactively on the application data without the involvement of a human annotator, as seen in Fig. 4.

¹<https://www.connectedpapers.com/>

TABLE I

ASSIGNMENT OF THE REVIEWED METHODS TO THEIR CORRESPONDING TAXONOMY NODES. APP: APPLICATION, SIM: SIMULATED, ITER: ITERATIVE

Paper	Year	Interaction	Guidance Signal	Taxonomy Node	Target	Modality	Paper Link
DeepCut [1]	2016	Bounding Box	GT Bounding Box	App Sim Non-Iter Rule-based	fetal brain, fetal lungs	MRI	Link
UI-Net [2]	2017	Scribbles	Error Skeletonization	App Sim Iter Uniform Error Sampling	liver lesions	CT	Link
Sun et al. [3]	2017	Clicks	Location Prior	App Sim Non-Iter Rule-based	prostate	MRI	Link
Can et al. [4]	2017	Scribbles	GT Scribbles	App Sim Non-Iter Rule-based	cardiac structures, prostate	MRI	Link
DeepGeoS [5]	2018	Scribbles	Geodesic Maps	App Sim Non-Iter Sampling-based	placenta, brain tumors	MRI	Link
BIFSeg [6]	2018	Scribbles	GT Scribbles	Online Fine-tuning	placenta, kidneys, fetal brain and lungs, brain tumors	MRI	Link
InterCNN [7]	2018	Scribbles	Subset of GT Mask	App Sim Iter Uniform Error Sampling	prostate	MRI	Link
Dhara et al. [8]	2018	Scribbles	GT Scribbles	Online Fine-tuning	brain tumors	MRI	Link
Tang et al. [9]	2018	Bounding Boxes	Implicit	App Sim Non-Iter Rule-based	lung nodules, liver lesions, lymph nodes	CT	Link
Sakinis et al. [10]	2019	Clicks	Gaussian Heatmaps	App Sim Iter Distance Transform-based Error Sampling	colon cancer, spleen, kidneys, gallbladder, esophagus, liver, stomach, blood vessels, pancreas, adrenal glands	CT	Link
Zhou et al. [11]	2019	Scribbles	GT Scribbles	App Sim Iter Rule-based Custom Rules	brain tumors	MRI	Link
Khan et al. [12]	2019	Clicks	Chebyshev Maps	App Sim Non-Iter Rule-based	heart, aorta, trachea, esophagus	CT	Link
DeepGeoSv2 [13]	2019	Scribbles	Euclidean Maps	App Sim Non-Iter Sampling-based	brain stem, parotid, optic nerve, optic chiasm	CT	Link
iW-Net [14]	2019	Clicks	Attraction Field Map	App Sim Non-Iter Rule-based	lung nodules	CT	Link
Roth et al. [15]	2019	Clicks	Gaussian Heatmaps	App Sim Non-Iter Rule-based	liver, spleen, prostate, cardiac structures	CT, MRI, US	Link
Cerome et al. [16]	2019	Clicks	Disks	App Sim Non-Iter Rule-based	neuron cells	Microscopy	Link
Zheng et al. [17]	2019	Scribbles	Implicit	App Non-interactive Training Post-processing	pancreas	CT	Link
Chao et al. [18]	2019	Scribbles	Implicit	Online Fine-tuning	esophageal cancer	PET/CT	Link
Långkvist et al. [19]	2019	Full Slice Annotation	Subset of GT Mask	Online Full Training	lung structures	CT	Link
Wang et al. [20]	2019	Contour Correction	Polygon Vertices	App Sim Non-Iter Sampling-based	liver	CT	Link
Boers et al. [21]	2020	Scribbles	Implicit	Online Fine-tuning	pancreas	CT	Link
UGIR [22]	2020	Scribbles	Geodesic Maps	App Sim Non-Iter Sampling-based	fetal brain	MRI	Link
IterMRL [23]	2020	Clicks	Geodesic Maps	App Sim Iter Rule-based Error Center	brain tumors, cardiac structures, prostate	MRI	Link
Raju et al. [24]	2020	Clicks	Gaussian Heatmaps	App Sim Non-Iter Rule-based	liver	CT	Link
BS-IRIS [25]	2020	Clicks	Geodesic Maps	App Sim Iter Uniform Error Sampling	brain tumors, cardiac structures, prostate	MRI	Link
NuClick [26]	2020	Clicks + Scribbles	Disks + GT Skeletonization	App Sim Non-Iter Sampling-based	intestinal glands, cell nuclei, white blood cells	Microscopy	Link
Kitrungrotsakul et al. [27]	2020	Scribbles	Error Skeletonization	App Sim Iter Rule-based Error Skeletonization	liver	CT	Link
IRIS [28]	2020	Clicks	Implicit	App Non-interactive Training Post-processing	aorta	CTA	Link
Hu et al. [29]	2020	Clicks	Geodesic Maps	App Sim Iter Uniform Error Sampling	brain tumors	MRI, CT	Link
Tian et al. [30]	2020	Contour Correction	Polygon Vertices	App Sim Iter Rule-based Worst Slice Correction	prostate, cardiac structures	MRI	Link
Chao et al. [2 [31]	2020	Scribbles	Implicit	App Sim Iter Rule-based Worst Slice Correction	nasopharyngeal and esophageal cancer	PET/CT	Link
Tang et al. [2 [32]	2020	Clicks	Euclidean Maps + Disks	App Sim Non-Iter Sampling-based	lung nodules, liver lesions, lymph nodes	CT	Link
Jimbo et al. [33]	2020	Scribbles	Gaussian Heatmaps	App Sim Iter Rule-based Error Skeletonization	liver	CT	Link
Girum et al. [34]	2020	Clicks	Implicit	App Sim Non-Iter Rule-based	prostate, cardiac structures	CT, US	Link
Ho et al. [35]	2020	Scribbles	GT Scribbles	Train Active Learning	osteosarcoma	Microscopy	Link
Foo et al. [36]	2021	Scribbles	Lines	App Sim Iter Rule-based Error Center	COVID19 lesions	CT	Link
Menon et al. [37]	2021	Scribbles	Implicit	Train Active Learning	colorectal cancer, breast cancer	Microscopy	Link
MIDDeepSeg [38]	2021	Clicks	Exponential Geodesic Maps	App Sim Non-Iter Rule-based	placenta, spleen, kidney, prostate, fetal brain	CT, MRI, US	Link
Feng et al. [39]	2021	Clicks	Disks	App Sim Iter Rule-based Error Center	liver, kidney, stomach, breast	CT	Link
Roth et al. [2 [40]	2021	Clicks	Gaussian Heatmaps	App Sim Non-Iter Rule-based	spleen, liver, pancreas, kidneys, gallbladder	CT	Link
Sambaturu et al. [41]	2021	Scribbles	GT Scribbles	Online Fine-tuning	cell nuclei, liver, liver lesions, heart, trachea, aorta, esophagus, brain tumors	Microscopy, MRI, CT	Link
Zhou et al. [2 [42]	2021	Scribbles	GT Scribbles	App Non-interactive Training Pre-saved Weak Labels	lung, colon, kidney, kidney tumors	CT	Link
Williams et al. [43]	2021	Contour Correction	B-splines	App Non-interactive Training Post-processing	breast cancer	US	Link
WDTISeg [44]	2021	Clicks	Euclidean Maps + Geodesic Maps	App Sim Non-Iter Sampling-based	breast cancer	US	Link
Li et al. [45]	2021	Clicks	Gaussian Heatmaps	App Sim Iter Uniform Error Sampling	brain tumors, cardiac structures, spleen, liver	MRI, CT, CT/MRI	Link
Deng et al. [46]	2021	Scribbles	Implicit	App Sim Iter Uniform Error Sampling	aortic system, brain tumors	CTA, MRI	Link
Zhang et al. [47]	2021	Clicks	Implicit	App Sim Non-Iter Rule-based	kidney tumors, prostate	CT, MRI	Link
Zheng et al. [2 [48]	2021	Scribbles	Implicit	Online Fine-tuning	skin lesions	Dermoscopy	Link
DINs [49]	2021	Clicks	Gaussian Heatmaps	App Sim Iter Rule-based Error Center	neurofibromatosis type 1	MRI	Link
Tian et al. [2 [50]	2021	Contour Correction	Polygon Vertices	App Sim Iter Rule-based Worst Slice Correction	prostate, kidney, kidney tumors	MRI	Link
Jiang et al. [51]	2021	Clicks	Gaussian Heatmaps	App Sim Non-Iter Sampling-based	skin lesions	Dermoscopy	Link
Bai et al. [52]	2021	Clicks	Gaussian Heatmaps	App Sim Iter Prediction-based Error Sampling	cardiac structures, prostate, kidney, spleen, lung cancer, colon cancer, kidney cancer	CT, MRI	Link
DeepScribble [53]	2021	Scribbles	Euclidean Maps	App Sim Iter Rule-based Error Skeletonization	liver tumors	Microscopy	Link
Attention-RefNet [54]	2021	Scribbles	App Sim Iter Rule-based Error Skeletonization	COVID19 lesions	CT	Link	
Daultabad et al. [55]	2021	Clicks	Disks	App Sim Non-Iter Sampling-based	thyroid nodules	US	Link
Manh et al. [56]	2021	Clicks	Implicit	App Non-interactive Training Post-processing	Z-line	Colonoscopy	Link
Trimpi et al. [57]	2021	Full Slice Annotation	Subset of GT Mask	App Sim Non-Iter Rule-based	heart, esophagus, lungs, spinal cord, lung tumors, pancreas, pancreas tumors, liver, liver tumors, neck, submandibular gland, parotid, brain, brain tumors, spleen	CT	Link
PIPo-Net [58]	2021	Contour Correction	Polygon Vertices	App Non-interactive Training Post-processing	breast cancer	Microscopy	Link
Jahanifar et al. [59]	2021	Scribbles	GT Skeletonization	App Sim Non-Iter Rule-based	breast cancer	Microscopy	Link
Sun et al. [2 [60]	2022	Contour Correction	B-splines	App Non-interactive Training Post-processing	prostate, nasopharyngeal cancer	MRI	Link
Shahedi et al. [61]	2022	Clicks	Disks	App Sim Non-Iter Sampling-based	prostate, kidney, kidney tumors	MRI	Link
Atzeni et al. [62]	2022	Scribbles	Implicit	Train Active Learning	brain structures	MRI, Microscopy	Link
Bi et al. [63]	2022	Clicks	Euclidean Maps	App Sim Non-Iter Sampling-based	skin lesions	Dermoscopy	Link
iSegFormer [64]	2022	Clicks	Disks	App Sim Iter Rule-based Error Center	knee cartilage	MRI	Link
ECONet [65]	2022	Scribbles	GT Scribbles	Online Full Training	COVID19 lesions	CT	Link
i3Deep [66]	2022	Scribbles	Subset of GT Mask	App Sim Non-Iter Sampling-based	brain tumors, pancreas, COVID19 lesions	CT, MRI	Link
DeepEdin [67]	2022	Clicks	Gaussian Heatmaps	App Sim Iter Prediction-based Error Sampling	prostate, prostate tumors	MRI, CT, CT/MRI	Link
Liu et al. [68]	2022	Clicks	Disks	App Sim Iter Rule-based Error Center	lung cancer, pancreas	MRI	Link
Shi et al. [69]	2022	Scribbles	Error Skeletonization	App Sim Non-Iter Sampling-based	colon cancer, lung cancer, kidney tumors, kidney	CT	Link
AnatomySketch [70]	2022	Scribbles + Contour Correction	GT Scribbles + B-Splines	Train Active Learning	liver cancer, lung lobes, intervertebral disc	MRI, CT	Link
Galisot et al. [71]	2022	Bounding Boxes	Implicit	App Sim Non-Iter Rule-based	brain structures	MRI	Link
Lin et al. [72]	2022	Scribbles + Clicks + Bounding Boxes	Gaussian Heatmaps + BBox Mask	App Sim Iter Rule-based Custom Rules	COVID19 lesions, brain tumors, brachial plexus, polyps, skin lesions	X-Ray, CT, MRI, US, Colonoscopy	Link
Pirabakaran et al. [73]	2022	Clicks	Gaussian Heatmaps	App Sim Non-Iter Sampling-based	spleen, colon cancer	CT	Link
Mikhailov et al. [74]	2022	Clicks	Disks	App Sim Iter Uniform Error Sampling	uterus, bladder, uterine cavity, female pelvis tumors	MRI	Link
Pirabakaran et al. [2 [75]	2022	Clicks	Gaussian Heatmaps	App Sim Non-Iter Sampling-based	spleen, colon cancer	CT	Link
Chen et al. [76]	2022	Clicks	Gaussian Heatmaps + Euclidean Maps	App Sim Non-Iter Rule-based	breast lesions	US	Link
Deep SED-Net [77]	2022	Scribbles	GT Scribbles	Train Active Learning	testicular cells	Microscopy	Link
Ju et al. [78]	2022	Clicks	Implicit	App Sim Non-Iter Sampling-based	liver, kidneys, spleen	CT	Link
Ma et al. [79]	2022	Scribbles	Implicit	Train Active Learning	liver, spleen	CT, MRI	Link
Bai et al. [2 [80]	2022	Clicks	Gaussian Heatmaps	App Sim Iter Prediction-based Error Sampling	nasopharyngeal cancer	CT	Link
Zhou et al. [3 [81]	2023	Scribbles	Geodesic Maps	App Non-interactive Training Pre-saved Weak Labels	lung, colon, kidney, kidney tumors	CT, Colonoscopy	Link
Hallitschke et al. [82]	2023	Scribbles	Geodesic Maps	App Sim Non-Iter Sampling-based	lung cancer	PET/CT	Link
Liu et al. [2 [83]	2023	Clicks + Scribbles	Disks + GT Scribbles	App Sim Iter Rule-based Error Center	esophagus, cardiac structures, pancreas, celiac trunk, spleen, gallbladder, stomach, kidney, liver, aorta, ribs, femoral cartilage	CT	Link
Bruzadin et al. [84]	2023	Scribbles	Implicit	App Sim Non-Iter Rule-based	COVID19 lesions	CT	Link
Asad et al. [85]	2023	Scribbles	GT Scribbles	Online Full Training	COVID19 lesions	CT	Link
Shahin et al. [86]	2023	Scribbles	Gaussian Heatmaps	App Sim Non-Iter Rule-based	cardiac structures	US	Link
Zhuang et al. [87]	2023	Contour Correction	Polygon Vertices	Train Active Learning	liver, spleen, kidneys	CT	Link
Ho et al. [2 [88]	2023	Scribbles	GT Scribbles	Train Active Learning	ovarian cancer	Microscopy	Link
Wei et al. [2 [89]	2023	Scribbles	GT Scribbles	App Sim Iter Rule-based Worst Slice Correction	head-and-neck cancer	PET/CT/MRI	Link
Zhuang et al. [2 [90]	2023	Scribbles	Exponential Geodesic Maps	Train Active Learning	lung tumors, liver tumors	CT, MRI	Link
GiG [91]	2023	Clicks	Gaussian Heatmaps	Sim Iter Distance Transform-based Sampling	lung lesions, lymphoma, melanoma, spleen	CT, PET/CT	Link
Qu et al. [92]	2023	Scribbles	Subset of GT Mask	Train Active Learning	spleen, liver, kidneys, stomach, gallbladder, pancreas, aorta, cardiac structures	CT	Link

Ho et al. [35] pioneer the use of active learning in the field of deep medical interactive segmentation by applying a Convolutional Neural Network (CNN) on an unlabeled osteosarcoma dataset reducing the annotation time significantly compared to standard pixelwise annotation. Menon et al. [37] ask the annotator to highlight a query patch for the annotation of a whole-slide image (WSI). A retrieval module chooses the K-nearest patches in the image to the query patch by

assessing their similarity in the feature space. The annotator then provides feedback for each patch, either as relevant or irrelevant, or provides explicit segmentation labels. This way, only the most informative patches are annotated and Menon et al. [37] show that using their retrieval module, only 5% of the patches need to be annotated to achieve state-of-the-art performance. Atzeni et al. [62] introduce a method that leverages estimated segmentation quality and labeling effort

TABLE II
ASSIGNMENT OF SAM-BASED [137] METHODS TO THEIR TAXONOMY NODES. APP: APPLICATION, SIM: SIMULATED, ITER: ITERATIVE

Paper	Year	Interaction	Guidance Signal	Taxonomy Node	Target	Modality	Paper Link
Mazurowski et al. [93]	2023	Clicks + Bounding Boxes	Positional Encoding	App Sim Iter Uniform Error Sampling	gray matter, spinal cord, heart, prostate, brain tumors, breasts, female genital tract, chest, ilium, femur, kidney, muscle, nerves, ovarian tumors, colon cancer, vessels, spleen, liver, bladder, lungs, lung cancer, melanoma, lymphoma	CT, MRI, US, X-Ray, PET/CT	Link
Deng et al. [94]	2023	Clicks + Bounding Boxes	Positional Encoding	App Sim Iter Uniform Error Sampling	cell nuclei, skin cancer	Microscopy	Link
SAM vs. BET [95]	2023	Clicks + Bounding Boxes	Positional Encoding	App Sim Iter Uniform Error Sampling	brain	MRI	Link
Putz et al. [96]	2023	Clicks + Bounding Boxes	Positional Encoding	App Sim Iter Uniform Error Sampling	brain tumors	MRI	Link
Hu et al. [97]	2023	Clicks + Bounding Boxes	Positional Encoding	App Sim Iter Uniform Error Sampling	liver tumors	CT	Link
SAM-Adapter [98]	2023	Clicks + Bounding Boxes	Positional Encoding	App Sim Iter Uniform Error Sampling	polyps	Colonoscopy	Link
Medical SAM Adapter [99]	2023	Clicks	Positional Encoding	App Sim Iter Uniform Error Sampling	spleen, kidneys, gallbladder, esophagus, liver, stomach, aorta, cardiac structures, pancreas, adrenal glands, duodenum, bladder, optic cup, brain tumors, thyroid nodules	CT, MRI, US, Fundus, Dermoscopy	Link
Ophthalmology SAM [100]	2023	Clicks + Bounding Boxes	Positional Encoding	App Sim Iter Uniform Error Sampling	blood vessels, retinal lesions	Fundus	Link
He et al. [101]	2023	Clicks + Bounding Boxes	Positional Encoding	App Sim Iter Uniform Error Sampling	heart, brain, breasts, lung, bowel, pancreas, prostate, skin, heart, liver, brain, chest	MRI, US, CT, Colonoscopy, Dermoscopy, X-Ray	Link
Shi et al. [102]	2023	Clicks + Bounding Boxes	Positional Encoding	App Sim Iter Uniform Error Sampling	skin, eyes, chest, colon, retina, abdominal organs	Colonoscopy, Fundus, CT, MRI, Colonoscopy, X-Ray, OCT	Link
GazeSAM [103]	2023	Eye Gaze	Positional Encoding	App Sim Iter Uniform Error Sampling	not specified	not specified	Link
SkinSAM [104]	2023	Bounding Boxes	Positional Encoding	App Sim Iter Uniform Error Sampling	skin lesions	Dermoscopy	Link
Wang et al. [105]	2023	Clicks + Bounding Boxes	Positional Encoding	App Sim Iter Uniform Error Sampling	surgery instruments	Colonoscopy	Link
Cheng et al. [106]	2023	Clicks + Bounding Boxes	Positional Encoding	App Sim Iter Uniform Error Sampling	breasts, polyps, foot ulcers, COVID19 lesions, hippocampus, thyroid nodules, thyroid gland, liver tumors	US, Colonoscopy, MRI, CT	Link
Mattjie et al. [107]	2023	Clicks + Bounding Boxes	Positional Encoding	App Sim Iter Uniform Error Sampling	skin lesions, lungs, femur, ilium, polyps, breasts	X-Ray, US, Colonoscopy, Dermoscopy	Link
PolypSAM [108]	2023	Bounding Boxes	Positional Encoding	App Sim Iter Uniform Error Sampling	polyps	Colonoscopy	Link
PromptUNet [109]	2023	Clicks + Bounding Boxes + Scribbles	Positional Encoding + Subset of GT Mask	App Sim Iter Uniform Error Sampling	spleen, kidneys, gallbladder, esophagus, liver, stomach, aorta, cardiac structures, pancreas, adrenal glands, duodenum, bladder, optic cup, brain tumors, thyroid nodules	CT, MRI, US, Fundus, Dermoscopy	Link
BreastSAM [110]	2023	Clicks + Bounding Boxes	Positional Encoding	App Sim Iter Uniform Error Sampling	breast cancer	US	Link
IAMSAM [111]	2023	Clicks + Bounding Boxes	Positional Encoding	App Sim Iter Uniform Error Sampling	breast cancer, colon, brain, prostate cancer,	Microscopy	Link
DeSAM [112]	2023	Clicks + Bounding Boxes	Positional Encoding	App Sim Iter Uniform Error Sampling	prostate	MRI	Link
Shen et al. [113]	2023	Clicks + Bounding Boxes	Positional Encoding	App Sim Iter Uniform Error Sampling	brain tumors	MRI	Link
Ning et al. [114]	2023	Clicks + Bounding Boxes	Positional Encoding	App Sim Iter Uniform Error Sampling	heart, thyroid, carotid artery	US	Link
Zhang et al. [115]	2023	Clicks + Bounding Boxes	Positional Encoding	App Sim Iter Uniform Error Sampling	prostate, bladder, femoral heads, rectum, lungs, heart, spinal cord, esophagus, liver, stomach, kidneys, large and small bowels, brain, parotids, mandible, cochleas	CT	Link
MedLSAM [116]	2023	Clicks + Bounding Boxes	Positional Encoding	App Sim Iter Uniform Error Sampling	liver, spleen, kidneys, stomach, gallbladder, esophagus, pancreas, duodenum, colon, intestines, adrenal gland, rectum, bladder, femur heads, brain stem, eyes, lens, optic nerve, optic chiasm, brain structures, pituitary gland, parotids, cochlea, spinal chord, mandibles	CT	Link
SAM-U [117]	2023	Bounding Boxes	Positional Encoding	App Sim Iter Uniform Error Sampling	optic disc, optic cup	Fundus	Link
3DSAM-adapter [118]	2023	Clicks	Positional Encoding	App Sim Iter Uniform Error Sampling	liver tumors, kidney tumors, pancreas tumors, colon cancer	CT	Link
Huang and Yang et al. [119]	2023	Clicks + Bounding Boxes	Positional Encoding	App Sim Iter Uniform Error Sampling	See [119, Table 2] for a comprehensive list of all 68 targets	CT, MRI, Colonoscopy, US, Fundus, Microscopy, Colonoscopy, X-Ray	Link
MedSAM [120]	2023	Clicks + Bounding Boxes	Positional Encoding	App Sim Iter Uniform Error Sampling	See Tables 1-4 in MedSAM's supplementary material (link) for a comprehensive list of all >60 targets	CT, MRI, US, X-Ray, PET/CT, Microscopy, OCT, Colonoscopy, Fundus	Link
SAM.MD [121]	2023	Clicks + Bounding Boxes	Positional Encoding	App Sim Iter Uniform Error Sampling	spleen, kidneys, gallbladder, esophagus, liver, stomach, aorta, postcava, pancreas, adrenal glands, duodenum, bladder	CT	Link

to identify regions of interest effectively. The labeling effort is based on the boundary length and its irregularity, assuming that large structures with complex boundaries are difficult to annotate. The segmentation quality is measured by the average class Dice score on already annotated regions. As a result, easier regions can be selected for annotation in the initial rounds enabling the model to acquire valuable features that prove beneficial for annotating more challenging areas at later stages. AnatomySketch [70] presents an open-source software platform with a graphical user interface designed for annotating and integrating deep learning segmentation models. The "Annotation-by-iterative-Deep-Learning (AIDL)" module enables annotators to proofread, correct, and incorporate segmentations into the next training iteration of a pre-trained model. Deep SED-Net [77] demonstrates how an AIDL strategy for testicular cell segmentation achieves the same results as manual annotation using squeeze-and-excitation layers [130] in a U-Net model [127]. Ma et al. [79] utilize an igniter network trained on a small dataset to generate coarse labels on a larger dataset for a bigger model. The larger model is trained in an AIDL loop, involving a human annotator following a specific labeling protocol. The protocol prioritizes easier samples for early labeling and gradually addresses harder samples in subsequent iterations, effectively minimizing human effort while improving the larger model's final predictions on the challenging samples, similar to Atzeni et al. [62]. Zhuang et al. [87] introduce a boundary contour correction tool as an alternative to voxel-wise corrections. Their approach demonstrates improved shape learning, faster proofreading, and more anatomically plausible results, showcasing the benefits of using a contour representation. Ho et al. [88] further accelerate the AIDL paradigm by employing

a pre-trained breast segmentation model instead of using random weight initialization, resulting in reduced annotation time. Zhuang et al. [90] utilize user-provided scribbles to compute an exponentialized geodesic distance map, which is then used to modulate the model's prediction. This process generates pseudo-labels for the subsequent training iteration. The pseudo-labels are implicitly more certain near the scribbles and incorporate human feedback during training. Qu et al. [92] train three models (U-Net [127], Swin-UNETR [135], and nnU-Net [136]) on a small CT dataset and use these models to annotate 8000 CT volumes. They use the inconsistency between the three models' predictions, the prediction entropy, and the overlap of model predictions to suggest volumes for refinement to the annotator. They show the three metrics correlate highly with error regions, i.e., can identify which volumes are the most informative to refine and reduce the annotation time of 8000 CTs to two work weeks [92].

B. Application Only

The second category of our taxonomy encompasses models engaging with human annotators exclusively during the application stage, depicted as green and red nodes in Fig. 3. During the training stage, these models either: 1) utilize simulated interactions generated by a simulated annotator (green nodes), often referred to as a *robot user* in literature [122]; or 2) have no interactions (red nodes). During the application stage, human users interact with these models by providing initial and/or iterative corrective interactions.

1) *Simulated Training Interactions*: To circumvent the need for human annotators during the training process, one approach is to simulate the annotation process using a *robot user*. This

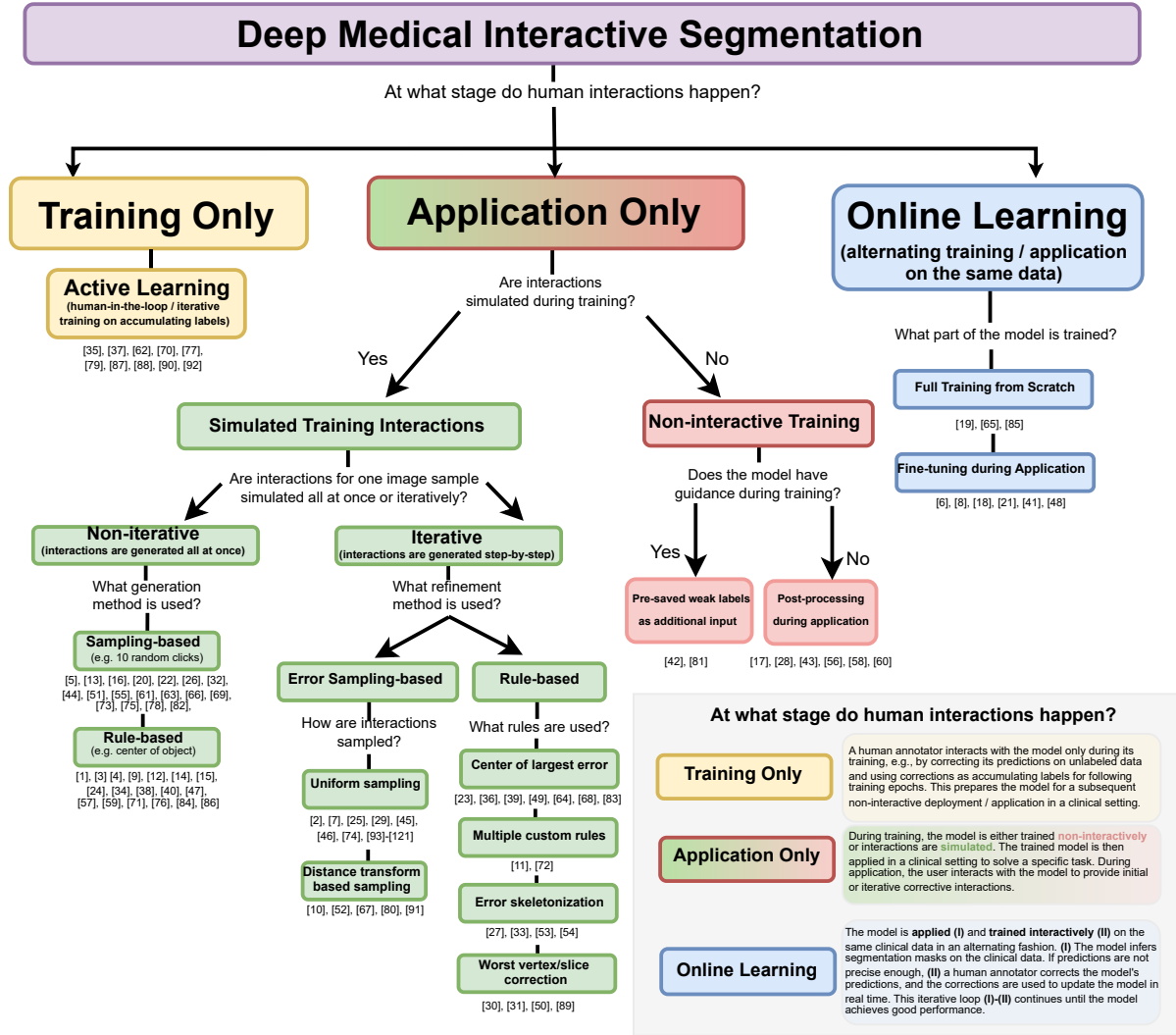


Fig. 3. Our proposed taxonomy tree for all the reviewed studies. The references for studies associated with a node are listed beneath the respective node.

robot user mimics the behavior of a human annotator and relies on ground truth labels to simulate interactions only in the correct regions. In our taxonomy, we differentiate between iterative and non-iterative simulation.

1a) *Non-iterative simulation*: In the non-iterative simulation, interactions are generated all at once in a single iteration and then transformed into a guidance signal, which is combined with the image. During training, there are no correction loops, whereas during the application stage, human annotators can iteratively correct the model's predictions, as illustrated in Fig. 4. Non-iterative methods can be further subdivided into the two subcategories *rule-based* and *sampling-based*, depending on whether the interactions are generated through deterministic rules (e.g., the center of the largest connected component in the mask) or by randomly sampling the ground-truth mask, respectively.

Non-iterative rule-based methods employ deterministic rules to simulate interactions. For instance, Sun et al. [3] simulate a click by using the center of the prostate. They utilize the Canny edge detector [123] to generate horizontal and vertical location prior maps. These maps assign decreasing

intensity values to voxels that are farther from the central click and have more edges crossed (an example is given in the Appendixes). Khan et al. [12] utilize the extreme points of the object (topmost, leftmost, rightmost, and bottom-most points) as four clicks and generate a confidence map based on the Chebyshev and Mahalanobis distances to the center of the object. DeepCut [1] extends the ground-truth bounding box to generate foreground and background voxels, which serve as inputs for an interactive CNN. After that, dense CRFs [166] refine the CNN's predictions, and the refined predictions from the dense CRFs are utilized again as the foreground and background voxel seeds for the interactive CNN. Can et al. [4] also utilize dense CRFs to refine CNN predictions for prostate and cardiac structures segmentation. iW-Net [14] simulates two clicks by selecting the two farthest points in the ground truth mask. These two points are used to compute an attraction field, inspired by the punctual electric charges of opposite values (an example is given in the Appendixes). Roth et al. [15], [40] utilize 3D Gaussian heatmaps centered at the extreme points which are subsequently expanded and

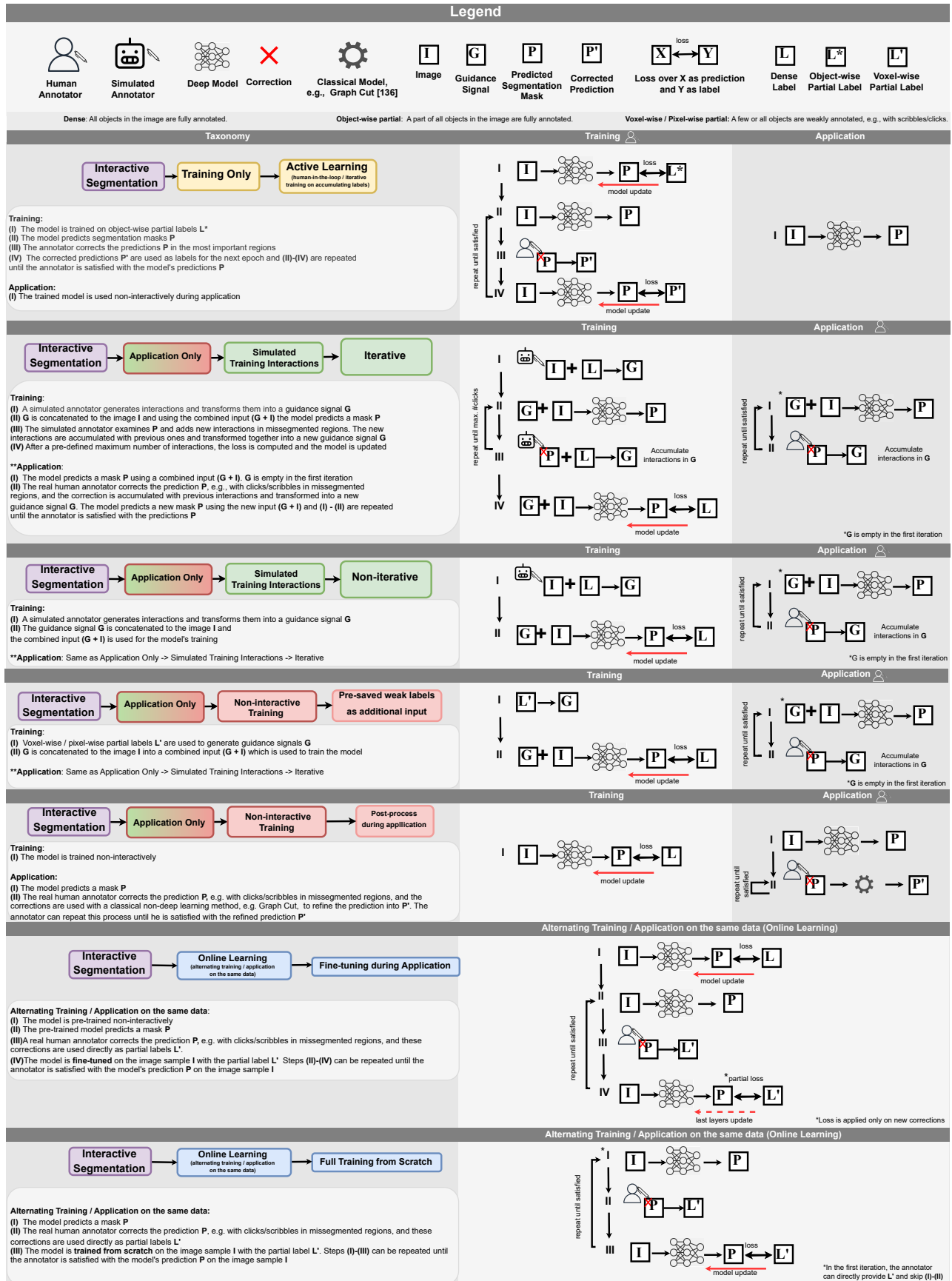


Fig. 4. Taxonomy blueprints for our proposed taxonomy nodes. The human annotator is involved during training, application, or both in *online learning*.

used as a guidance signal for a CNN-based model. Raju et al. [24] tackle the domain gap between simulated and ground-truth extreme points by training a model to predict these points on unseen data and utilize them as a guidance signal. Girum et al. [34] also employ extreme points as input to their prior-knowledge network. Their network generates a spatial attention map that is then multiplied with the image and fed into a downstream segmentation model. MIDeepSeg [38] leverages extreme points to simulate clicks and slightly shifts them towards the inner side of the boundary to obtain interior margin points. These points are then used to compute an exponentialized geodesic distance map as a guidance signal. Zhang et al. [47] extract image patches along rays extending from the object’s center to its outer boundaries, which are then used to train a Convolutional Recurrent Neural Network (ConvRNN) model. In the application stage, a single click at the object’s center is sufficient, as the ConvRNN model sequentially segments the neighboring patches around the click. Trimpl et al. [57] simulate the complete annotation of the central axial slice in a CT image and propagate it to the remaining slices in the volume. Their model leverages the central slice, its annotation, and a target slice as joint inputs to learn the segmentation of the target slice. The entire volume is segmented by iteratively choosing each slice from the CT as a new target slice. Jahanifar et al. [59] skeletonize the ground-truth mask to produce simulated scribbles. i3Deep [66] randomly samples multiple slices from the ground-truth labels for each image sample. The full image labels of the selected slices are then appended to the input of a refinement model during the training stage. Galisot et al. [71] train segmentation models on a variety of brain structures using cropped regions from the entire brain as inputs. Moreover, they develop a model to learn spatial relationships between structures, automatically positioning bounding boxes during inference, and allowing annotators to adjust the bounding boxes as needed. Chen et al. [76] generate 2D Gaussian heatmaps around each extreme point and compute an Euclidean distance transform using the intersection point of the two extreme axes as a seed point to produce a second guidance signal. Bruzadin et al. [84] propagate foreground seeds from a source slice to neighboring slices by considering the strong edges in the image and avoiding sampling seeds near those edges in the adjacent slices. Shahin et al. [86] identify the slice with the highest error and use the ground-truth boundary of that slice as a simulated scribble.

Non-iterative sampling-based methods sample the ground-truth labels to simulate interactions. DeepIGeoS [5] samples a fixed amount of voxels from connected components that are over a certain size threshold and uses them as seeds for computing a geodesic distance transform. UGIR [22], Bi et al. [63], DeepIGeoSv2 [13], WDTISeg [44], and Hallitschke et al. [82] follow the same sampling strategy as DeepIGeoS [5]. UGIR [22] additionally estimates the segmentation uncertainty by calculating the prediction variance within a group convolution layer. Bi et al. [63] integrate the guidance signal at multiple stages in their skin lesion segmentation model. DeepIGeoSv2 [13] expands upon the two-stage DeepIGeoS [5] model to handle multiple organs and introduces an uncertainty-

aware loss function that assigns an exponential penalty based on the model’s certainty of an error. WDTISeg [44] combines geodesic and Euclidean distance maps through a linear combination, allowing the incorporation of both appearance and location information, respectively. Hallitschke et al. [82] extend DeepIGeoS [5] to multimodal PET/CT data and investigate different ways to present the annotation interface to the user when displaying multimodal data for annotation. Cerrone et al. [16] segment neuron cells from serial section electron microscopy images by randomly sampling a click from each neuron in the image while enforcing a minimum distance to any boundary. Wang et al. [20] perturb the vertices of the ground-truth polygon of the object’s boundary by applying randomly sampled offsets and directions. NuClick [26] randomly samples a point inside each nucleus so that it is at least two pixels away from the object boundaries. Tang et al. [32] perform dilation on the ground-truth masks of liver and lung lesions as well as lymph nodes, and then randomly sample five pixels from the dilated mask. Jiang et al. [51] adopt a two-stage network approach and randomly sample clicks from the segmentation error of the first-stage coarse network, encoding them as Gaussian heatmaps. Daulatabad et al. [55] sample multiple clicks in the proximity of the centroid of the ground-truth mask of the thyroid nodule. Shi et al. [69] partition the ground-truth mask into sections based on the Euclidean distance to the object’s boundary. Subsequently, one random pixel is sampled from each section. This technique mitigates the issue of cluttered samples that are in close proximity to each other in the guidance map. Shahedi et al. [61] and Ju et al. [78] uniformly sample clicks from the target organ. Both methods experiment with different numbers of sampled clicks in their ablations studies. Pirabaharan et al. [73], [75] uniformly sample the ground-truth mask to generate foreground and background clicks. These clicks are encoded using Gaussian heatmaps, where the radius of each heatmap is proportional to the area of the corresponding ground-truth mask. The heatmaps exhibit smaller radii for smaller objects, allowing them to align more accurately with their boundaries.

b) Iterative simulation: Iterative simulation methods mimic the iterative nature of interaction segmentation during application where the human annotator repeatedly corrects the prediction on the model in a typical human-in-the-loop scenario. This loop is simulated by either sampling interactions from the missegmented regions or defining deterministic rules to choose each next interaction, e.g., choosing the center of the largest erroneous region.

Iterative error sampling-based methods sample interactions for the next iteration from missegmented regions. We distinguish between uniform and distance transform-based sampling in our taxonomy, depending on how interactions are sampled.

Iterative uniform sampling approaches sample new interactions with an equal probability of landing in any of the missegmented pixels/voxels. UI-Net [2] identifies the missegmented regions of hepatic lesions and samples a random number of pixels for each interaction. For the first interaction, they initialize the foreground and background scribbles by performing multiple dilation and erosion operations on the lesion’s boundary, respectively. InterCNN [7] uniformly samples multiple

clicks from the error, places a 9×9 window around each click, and adds all foreground pixels in the window to the sampled clicks, regardless of whether they were missegmented. Hu et al. [29] use a stratification approach, randomly sampling a click from each of the three largest missegmented connected components. Li et al. [45] randomly sample clicks from the intersection area between the object’s boundary and the error regions. They adopt a reinforcement learning approach, where the agent is rewarded based on the cross-entropy improvement. They also propose a confidence estimation network that guides the human annotator during application by suggesting click locations based on the segmentation confidence. Deng et al. [46] adopt a sampling strategy where a fixed number of under- and oversegmented voxels are selected at each iteration. Their loss function exclusively focuses on the $9 \times 9 \times 9$ neighborhood surrounding each missegmented voxel to avoid contaminating the already well-segmented regions. Mikhailov et al. [74] randomly sample clicks from missegmented regions and store the sampled clicks from all iterations in an ordered memory bank. The memory bank preserves the sequence of interactions instead of combining all the clicks into a single guidance signal, ensuring that the sequential information is retained.

Recently, Meta AI released the code for their Segment Anything Model (SAM) [137]. Due to its remarkable performance and zero-shot capabilities on natural images, many methods have adapted SAM for medical images. In this review, we only consider methods that use SAM’s interactive prompts. All the reviewed medical SAM methods fall into the category of iterative uniform sampling simulation in our taxonomy, which uses SAM’s original pre-training described in the training algorithm in [137, p.17]. Here, we summarize these methods.

Mazurowski et al. [93] extensively evaluate the zero-shot performance of SAM on 33 datasets and observe significant performance variations across different tasks, ranging from 0.11 to 0.86 Intersection over Union. Their findings highlight that bounding box prompts consistently yield superior results and that SAM performs better on larger objects. Interestingly, the study demonstrates that iterative corrections do not lead to substantial improvements, with the best performance achieved in the first three clicks for most tasks. Deng et al. [94] similarly conclude that SAM excels in segmenting larger objects but faces challenges when dealing with multiple small objects, even with an abundance of prompts. The study highlights that SAM is unsuitable for gigapixel WSI data. SAM vs. BET [95] exhibits SAM’s superior performance over the gold standard Brain Extraction Tool (BET) [134] in brain extraction from Magnetic Resonance Imaging (MRI) images but it does not compare it to more recent skull stripping models [101]. Putz et al. [96] demonstrate SAM’s effective generalization in glioma brain tumor segmentation, except for small tumors under 300 mm^3 , where its performance shows some deterioration. Hu et al. [97] examine SAM’s effectiveness in liver tumor segmentation, but the study concludes that there exists a considerable performance gap compared to even a simple U-Net model [127]. SAM-Adapter [98] incorporates task-specific knowledge by injecting task-specific embeddings into SAM’s image encoder which leads to a significant improvement in SAM’s performance for polyp segmentation compared to using

it directly without any modifications. Ophthalmology SAM [100] fine-tunes SAM with an additional prompt adapter on fundus images and improves SAM significantly on three ophthalmology tasks.

He et al. [101] evaluate SAM on 12 public medical datasets spanning ten organs and six imaging modalities. Their findings reveal that SAM is consistently outperformed by a simple U-Net [127] across all 12 datasets, and its performance is notably influenced by the size of the target object. Moreover, SAM achieves notably higher results on 2D modalities (dermoscopy, colonoscopy, X-Ray, ultrasound) when compared to 3D modalities such as MRI and CT. Shi et al. [102] confirm that SAM is easily outperformed by a simple U-Net model [127] in fundus, CT, MRI, and Optical Coherence Tomography (OCT) data. Nonetheless, they showcase that through in-domain fine-tuning, SAM reaches the performance level of specialized U-Net models in retinal vessel segmentation. GazeSAM [103] employs eye gazing to estimate the annotator’s point of focus, encodes these positions as clicks, and utilizes SAM for segmentation. SkinSAM [104] fine-tunes SAM on dermoscopy images by using simulated bounding box prompts, resulting in satisfying performance on skin lesion segmentation. Wang et al. [105] utilize SAM for surgical instrument segmentation and find that bounding box-based prompting outperforms click prompts by a significant margin. However, SAM’s performance remains unsatisfactory in challenging scenarios, such as dealing with overlapping instruments and blood. Cheng et al. [106] assess SAM without fine-tuning on 12 medical datasets, demonstrating that bounding boxes yield significantly better results compared to clicks. Additionally, the study finds that incorporating perturbations into the bounding boxes leads to a deterioration in performance. Mattjie et al. [107] investigate SAM across six datasets and affirm that employing the ground-truth bounding box without perturbations yields the best results consistently across all datasets and across various transformer backbones of SAM. Polyp-SAM [108] fine-tunes SAM on five colonoscopy datasets using bounding box prompts. They find that fine-tuning only the decoder instead of the whole model and using a smaller transformer backbone achieves the best performance. BreastSAM [110] also concludes that using a smaller transformer backbone leads to better results for breast cancer segmentation in ultrasound images. IAMSAM [111] implements an annotation interface for microscopy images where the segmentation masks are utilized for downstream tasks, such as cell type prediction and spatial transcriptomics. Shen et al. [113] extend SAM by incorporating temporal prompts, where a Reinforcement Learning (RL) agent suggests the appropriate type of prompt, such as a bounding box or click. The study demonstrates that the learned RL suggestions outperform choosing only one of the types of interaction. Ning et al. [114] apply SAM to ultrasound videos and unveil its potential for segmenting various structures, showcasing minimal deviations between video frames when sufficient prompts are provided. Zhang et al. [115] conduct experiments on multiple anatomical structures and conclude that SAM performs most effectively on large structures like the liver and brain. However, its performance deteriorates when applied to smaller and ambiguous targets such as the parotid and

cochlea. MedLSAM [116] uses extreme points that implicitly define a bounding box prompt for SAM and reduce the annotation burden. SAM-U [117] generates multiple bounding box prompts for a single input image. By computing the entropy of the predictions obtained by using each bounding box in a separate forward pass, SAM-U estimates the aleatoric uncertainty. This uncertainty metric highlights challenging regions in the image that necessitate additional guidance from the annotator. 3DSAM-adapter [118] is the first to adapt SAM to 3D images and 3D prompts. This adaptation is achieved by freezing the pre-trained weights and extending each of SAM’s components to 3D. The patch embedding is extended using a 3D depth-wise convolution. The 3D position encoding is produced by summing the embedding from SAM’s original 2D lookup table with the embedding from a new depth lookup table. The attention block extends from $[B, H \times W, c]$ to $[B, H \times W \times D, c]$ queries, and the bottleneck replaces all 2D convolutions with 3D. Huang and Yang et al. [119] curate 52 public datasets to assess SAM’s “Segment Everything” mode and different click and bounding box prompts. Their evaluation reveals that SAM’s performance varies considerably across the datasets, even for the same structure in different modalities. Additionally, the study concludes that using bounding boxes leads to higher and more consistent performance compared to using clicks, and employing the “Segment Everything” mode yields the least favorable results.

In contrast to the predominantly negative findings in most other works that integrate SAM for medical images, MedSAM [120] achieves a remarkable performance on 14 unseen datasets, covering 50 target classes and seven imaging modalities, and even surpasses specialized nnU-Net [136] models on each of the target classes. This impressive outcome is the result of the careful curation of 84 existing public medical datasets for pre-training, leading to 1 090 486 medical image-mask pairs, and fine-tuning SAM on this large-scale medical dataset. The diversity of this dataset, spanning 15 imaging modalities, bolsters MedSAM’s strong generalization abilities and reveals the significant potential of using SAM for medical interactive segmentation. Furthermore, MedSAM [120] concludes that bounding box prompts perform the best, and they convert 3D images into 2D slices for training and evaluation. Medical Sam Adapter (MSA) [99] implements an adapter that extends to depth attention to account for the dimensionality reduction from 3D to 2D images in SAM’s training. They pre-train SAM on multiple large-scale medical datasets and show superior performance to MedSAM [120] but only when using clicks instead of bounding boxes. PromptUNet [109] proposes to use U-Net [127] as a backbone for all encoders and decoders in SAM instead of a Vision Transformer (ViT) [138]. PromptUNet [109] shows that this architecture change leads to a significant improvement, outperforming both click-based MedSAM [120] and MSA [99] on five datasets. DeSAM [112] disentangles the prompt from the image to avoid the influence of poor prompts and shows considerable improvement to MedSAM [120], even with bounding box prompts.

Iterative distance transform-based sampling approaches apply a distance transform over the missegmented regions, generating a distance map that serves as a sampling distri-

bution for new interactions. As a result, these approaches prioritize sampling new interactions primarily in the central regions of the connected components of the errors. Sakinis et al. [10] introduced an approach that applies the Chamfer distance transform to errors and use the distance map as a sampling distribution for foreground and background clicks in each iteration. Bai et al. [52] apply the Euclidean distance transform to the over- and undersegmented regions to create the background and foreground sampling distributions respectively. They exponentialize and normalize the distance maps to convert them to a pseudo-probability map. DeepEdit [67] adopts the same strategy as Sakinis et al. [10]. However, they also experiment with different proportions of interaction-free iterations where the model receives no clicks, i.e., an empty guidance signal. Bai et al [80] apply the Euclidean distance transform to the error regions, followed by a Softmax normalization to produce a pseudo-probability map to sample new clicks. Guiding the Guidance (GtG) [91] extends DeepEdit [67] and proposes a dynamic Gaussian heatmap that has a larger radius in homogeneous regions and a smaller radius near edges. They compare four existing guidance signals and propose five evaluation metrics to facilitate a more systematic comparison of interactive models.

Iterative rule-based approaches utilize a deterministic rule to generate an interaction at each iteration. We differentiate between four types of rules: 1) center of largest error; 2) error skeletonization; 3) worst vertex/slice correction; and 4) multiple custom rules.

Center of largest error. Several methods use the center of the largest error region as the next click with the assumption that it is the most intuitive choice. IterMRL [23] and BS-IRIS [25] employ multi-agent reinforcement learning where each voxel is an agent with a cross-entropy improvement reward. During each iteration, IterMRL [23] selects the center of the largest error region along with the centers of the other $N - 1$ largest connected components. Feng et al. [39] combine few-shot learning with interactive segmentation by using only a small set of annotated slices and assigning clicks only to them during training. New clicks at each iteration are placed in the center of the largest connected error component of these slices. DINs [49] position new clicks in the center of the largest error region and verify if it belongs to the ground-truth class. For concave error regions where the center is not part of the error, an additional step is performed. The error region is skeletonized, and the nearest point in the skeleton to the selected point is used as the final click location. This ensures accurate click placement even in concave error regions. iSegFormer [64] introduces a transformer-based interactive model for knee cartilage segmentation and samples a click at the center of the under- and oversegmentated regions. Liu et al. [68] also introduce a transformer-based architecture that expands beyond binary segmentation to handle multiple classes. To address missegmentation, their approach involves placing new clicks at the centers of the largest missegmented regions for each class separately. Liu et al. [83] incorporate cycle consistency to preserve the quality of the initial segmentation in the refinement steps. They simulate the initial click in the largest anatomical structure and refine only the worst segmented organ

with central clicks in the following steps.

Error skeletonization simulates iterative scribbles as an alternative to iterative clicks. Similar to the central error clicks, error skeletonization generates scribbles that are positioned in the central regions of the object. A visual example of error skeletonization is given in the Appendixes. Kitrungrotsakul et al. [27] simulate foreground and background scribbles through skeletonization of under- and oversegmented errors, respectively. They utilize an initial non-interactive model followed by a second-stage model that incorporates the generated scribbles as additional input. Jinbo et al. [33] build upon the work of Kitrungrotsakul et al. [27] by introducing an enhanced annotation interface. This interface allows users to draw scribbles while simultaneously visualizing the preliminary segmentation result. DeepScribble [53] computes Euclidean distance maps for the false positive and false negative regions. The distance maps are thresholded and skeletonized to simulate scribble-like annotations. Attention-RefNet [54] also adopts skeletonized errors to emulate scribbles. The guidance signal is computed by subtracting the geodesic distance maps of the foreground and background so that it assigns positive values to the foreground and negative values to the background.

Worst vertex/slice correction. Another deterministic rule for enhancing segmentation involves identifying and selecting the worst vertex or slice at each iteration and incorporating its ground-truth value as a guidance signal. Tian et al. [30] leverage this approach by predicting the boundary polygon vertices and simulating the user dragging the worst vertex towards its correct position. They utilize a Graph Convolutional Network (GCN) to propagate this information to the remaining vertices in the polygon and update the segmentation contour accordingly. Tian et al. [50] extend this approach by incorporating a local correction. They update only the $2 \times K$ neighboring vertices of the corrected vertex. By confining the update to the local neighborhood, the other parts of the contour remain preserved, preventing changes to already well-segmented regions. Chao et al. [31] adopt a similar approach, but instead of focusing on individual vertices, they target the worst segmented 2D slice. The corrections of the worst slice serve as a supervisory signal to update the bottleneck feature of the segmentation model, after which the model is applied again to the whole volume. Wei et al. [89] also simulate a slice correction and use the ground-truth label of the slice with the largest tumor area as a guidance signal. They compare this strategy to random slice corrections to show that their approach selects more informative slices.

Multiple custom rules. The last taxonomy tree node we assign to the green partition are methods that apply multiple custom rules that are specific to the application. Zhou et al. [11] apply different types of interactions and simulate them during training. They simulate a central click by eroding the largest connected component multiple times and then select the center from the remaining eroded pixels. They also simulate scribbles by selecting the worst segmented 2D slice and connecting the two farthest points in the largest error component. Lin et al. [72] simulate a boundary scribble by dilating the object’s boundary and simulate iterative clicks by placing a central click in the largest error.

2) *Non-interactive Training:* Several interactive methods opt to exclude interactions during the training stage and, instead, adopt a standard non-interactive training approach. These methods are marked in red in Fig. 3. Based on their approach, these methods either post-processing the model prediction during the application or incorporate additional weak labels during training.

2a) *Post-processing during application:* Some methods adopt non-interactive training and integrate post-processing techniques to combine model predictions with user interactions during application. For instance, Zheng et al. [17] employ shadow set theory [124] to extract all ground-truth masks from the training dataset, which are fully aligned with the human clicks on an unseen image during application. The extracted masks are averaged and fused with the model’s prediction for the unseen image, while the mask variance serves as an estimate of uncertainty. In IRIS [28], patches centered around user clicks are extracted from the full volume and fed into a pre-trained model. The final prediction is obtained by stitching together the resulting predictions from all patches in a post-processing step. Williams et al. [43] employ B-spline active surfaces [125] to calculate an active contour along the boundary of a CNN prediction. The user can modify the contour by dragging its control points, and the active contour is updated by minimizing the Yezzi energy [126] with respect to the pixel intensities. PiPo-Net [58] utilizes a two-stage model comprising a U-Net [127] to generate a pixelwise segmentation mask and a post-processing Long Short-Term Memory (LSTM) model [128] to produce a vertex polygon over the mask’s boundary. The polygon vertices are predicted in consecutive steps. During application, the user can correct vertices, and the LSTM model updates all consecutive vertices as a post-processing step. Manh et al. [56] use a U-Net [127] for Z-line segmentation, followed by post-processing with a Binary Partition Tree (BPT) [132]. Users mark superpixels [133] with foreground and background clicks, and the BPT resolves conflicts with the U-Net predictions based on the Euclidean distance to the labeled superpixels. Sun et al. [60] adopt a two-stage approach for boundary prediction. First, a CNN predicts the initial contour, and subsequently, a GCN is trained as a post-processing step to predict the offset of the predicted boundary vertices from the ground-truth boundary.

2b) *Pre-saved weak labels as additional input.* Some models utilize additional weak labels during training. However, instead of using the weak labels as supervisory signals as done in weakly supervised learning [129], the weak labels are transformed into guidance signals. Zhou et al. [42], [81] utilize weak labels in the form of scribbles on a single source slice and propagate the label information from the source slice to the rest of the volume using a memory-readout operation from a memory-encoder network.

C. Online Learning

The third category in the taxonomy tree encompasses methods that undergo real-time training or fine-tuning directly on the data they are finally applied to. Methods in this paradigm produce on-the-fly predictions and allow annotators

to make immediate corrections with minimal or no latency between corrections, model updates, and new predictions. In our taxonomy, we differentiate between full training and fine-tuning based on the number of updated model parameters.

1) *Full Training from Scratch*: Some models do not use any pre-training and are trained entirely on the data on which they are finally applied. These models use the user interactions as the only labels, update their parameters in real-time, and predict again so that the user can correct them again until they are satisfied with the prediction's quality. Långkvist et al. [19] present a real-time annotation tool designed for CT scans to segment pulmonary fibrosis by training CNNs from scratch using only human interactions as labels. Their study investigates the trade-off between accuracy and efficiency by examining the performance of small and large models in online learning. ECONet [65] utilizes a small CNN model with only one convolution layer. After the user draws a scribble, ECONet uses fixed-size patches centered around each voxel in the scribble for model updates by utilizing the provided scribbles directly as the ground-truth mask. After each weight update, the model is applied to the whole volume using sliding window inference for Coronavirus Disease 2019 (COVID-19) lung lesion segmentation. Asad et al. [85] extend ECONet [65] by proposing an adaptive loss that propagates the influence of scribbles to neighboring regions with similar features. They also prune voxels with predictions under a certain confidence threshold to discard uncertain samples during weight updates.

2) *Fine-tuning during Application*: The second option for online learning models is to utilize a pre-trained model and only fine-tune it on the application data using human interactions. BIFSeg [6] utilizes a user-provided bounding box to crop the target and generates an initial segmentation using a pre-trained model. The user then corrects the initial predictions using scribbles, and the model undergoes fine-tuning with a scribble-based weighted loss function. Dhara et al. [8] expand the fine-tuning step into an iterative loop, where the annotator corrects model predictions with scribble-based GraphCut [131]. These corrections are then used to update the model in real-time. Chao et al. [18] propagate user corrections on a slice to neighboring slices by updating the model with a loss function based on the distance to the corrected slice. Boers et al. [21] employ a loss function that assigns higher weights to voxels from user-provided scribbles that are missegmented, while other voxels are weighted based on their distance to the scribbles. Sambaturu et al. [41] showcase an efficient model-agnostic scheme for fine-tuning using user-based scribbles. They dilate the scribbles with region growing and introduce an L2 regularization term to update the model's weights. The L2 term ensures that the updated weights are not drastically different from the initial ones, promoting stability in the model's predictions during the fine-tuning process.

V. REVIEW FINDINGS

In this section, we present our findings on the prevalent trends observed during the review of the 121 reviewed papers. We delve into the implications of these trends and the potential factors contributing to them. Through this analysis, we aim to

provide a comprehensive depiction of the current landscape within the medical interactive segmentation domain.

A. Segmentation Targets, Imaging Modalities, and Evaluation Metrics

1) *Segmentation Targets*: We distinguish segmentation targets in two primary categories: 1) anatomical structures and cells; and 2) pathologies. The categorization depends on whether a method's primary focus is on specific anatomical structures, distinct pathologies, or both (noted in $n=7$ of all 121 studies). The number of methods per specific anatomy or pathology is depicted in Fig. 5. Prominent anatomical regions encompass the brain, prostate, and cardiac structures as well as abdominal organs featuring the liver, spleen, kidney, pancreas, stomach, and gallbladder. Thoracic organs are less prominent, including lungs, aorta, esophagus, and cardiac structures, and whole-body structures like bones and blood vessels. Further notable regions of interest which are combined in the "Other"-category encompass lymph nodes, the Z-line, spine, cartilage, and skin. Furthermore, techniques using microscopy and OCT data are predominantly geared towards cell segmentation, targeting blood cells, testicular cells, neurons, or cell nuclei.

Pathological targets exhibit notably less diversity compared to their anatomical counterparts. The prevalent pathologies tend to concentrate primarily within the brain ($n=21$) and liver regions ($n=12$), largely owing to the prominence of datasets like: 1) BraTS [162] for brain cancer; 2) as well as MSD [163] and LiTS [164] for liver cancer. Beyond brain and liver cancer, a few specific targets emerge as representative of certain imaging modalities. Notably, COVID-19 lung lesions stand out in X-Rays, while skin lesions take precedence in dermoscopy. Colon cancer and polyps serve as typical examples in colonoscopy imaging. Other relevant pathologies encompass lung, breast, kidney, and thyroid cancer. The "Other"-category consists of less frequently encountered targets such as head and neck cancer, cervical, pancreatic, prostatic, and esophageal cancer, hematomas, and foot ulcers.

2) *Imaging Modalities*: Radiological modalities, particularly CT ($n=65$) and MRI ($n=42$), dominate the imaging modalities and are featured in the most reviewed methods. This prevalence can be attributed to the existence of popular public datasets from segmentation challenge competitions like MSD [163] and BraTS [162]. These challenges frequently release their training data publicly, incentivizing the adoption of these imaging modalities in many approaches. Subsequent to CT and MRI, ultrasound is the choice for $n=18$ out of 121 approaches, frequently applied in cardiac imaging, mammography, or fetal ultrasound. Microscopy finds application in $n=15$ out of 121 reviewed methods, predominantly in pathology for tumor or cancer cell identification. Colonoscopy stands as an imaging modality exclusively dedicated to polyp and/or colon cancer segmentation. Dermoscopy, on the other hand, specializes in skin lesion segmentation. Less frequently encountered imaging modalities in interactive models encompass OCT, X-Ray, fundus imaging, and PET/CT. For a comprehensive listing of segmentation targets and imaging modalities utilized by each reviewed method, refer to Tables I and II.

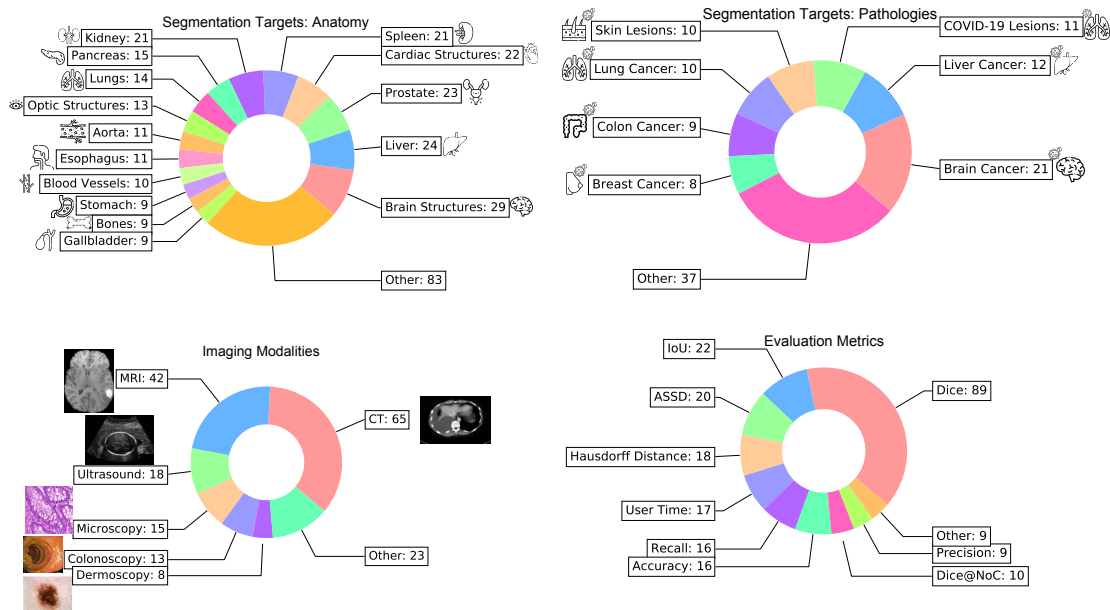


Fig. 5. Distribution of segmentation targets in the anatomy (top left) and in the pathology (top right), imaging modalities (bottom left), and evaluation metrics (bottom right) among all reviewed papers. The numbers represent the number of papers in that category. The icons on the top row are designed by Flaticon.com.

3) *Evaluation Metrics*: An adequate selection of evaluation metrics is crucial for meaningful assessment of segmentation methods, and thus, for trustworthy deployment in practice as well as scientific progress of the field. A large-scale investigation recently found that current medical image segmentation is subject to a substantial extent of pitfalls related to evaluation metrics [170]. The study reveals various shortcomings of the popular Dice Similarity Coefficient (DSC). At the same time, a follow-up study termed “Metrics Reloaded” provides a standardized framework for avoiding these pitfalls and selecting adequate metrics for a given problem [165]. One major finding was that performance should always be assessed by multiple metrics to account for failure modes such as of the DSC. Fig. 5 depicts the evaluation metrics employed by the reviewed studies. As expected, the most-used metric is DSC ($n=89$). However, oftentimes the DSC is the only reported metric for segmentation performance ($n=29$). Another common problem is the reporting of redundant metrics, such as reporting both DSC and Intersection over Union ($n=19$). Remarkably, despite its widespread use as a complementary metric to DSC in non-interactive segmentation and its endorsement by “Metrics Reloaded” for various settings, the Normalized Surface Distance [171] appears in only 2 out of 121 studies reviewed.

The incorporation of user-centered metrics is crucial for devising user-friendly and intuitive methods, particularly in the context of human-in-the-loop approaches. However, there is a noticeable scarcity of user-centric metrics in the reviewed studies. Some studies report the User Time ($n=17$), quantifying the active annotator’s labeling time in seconds, or the Dice@NoC ($n=10$), measuring the Dice score at a predefined Number of Clicks (NoC). Furthermore, the “Other”-category includes usability metrics like NASA-TLX [147] and the System Usability Scale [148], although these are seldom utilized.

B. Emergence of Foundation Models

In early 2023, the Segment Anything Model (SAM) [137] emerged, introducing an approach that involves large-scale training on over 1 billion segmentation masks. Although SAM’s initial training dataset (SA-1B) primarily comprises 2D natural images, several works have showcased its adaptability to medical data, spanning both 2D (such as dermoscopy and fundus) and 3D imaging modalities (including CT, MRI, and PET/CT). This versatility is achieved through targeted fine-tuning on medical data [120]. In the case of 3D images, it commonly involves using 2D axial slices [120] or integration of specialized 2D-to-3D adapters into the model [118].

SAM has shown a good generalization on multiple imaging modalities and tasks, especially on 2D modalities [120] utilizing its bounding box prompting capability. This lightweight adaptability has caused an unprecedented acceleration in the field of deep interactive medical image segmentation as evidenced by 29 proposed medical SAM-adaptations in only a few months at the time of writing. Thus, SAM has demonstrated the potential of utilizing foundation models for medical interactive segmentation. Further, due to its generalization and zero-shot capabilities, it seems to foster a trend towards evaluating methods on a larger number of tasks as some SAM-based approaches are evaluated on over 30 public medical datasets [119], [120].

C. Reproducibility and Availability

In recent years, the field of interactive medical segmentation has witnessed a surge in the emergence of new approaches. There is a promising shift towards enhanced reproducibility, with an increasing number of research papers releasing their code, often accompanied by detailed instructions for replicating results, and in some instances, providing pre-trained model

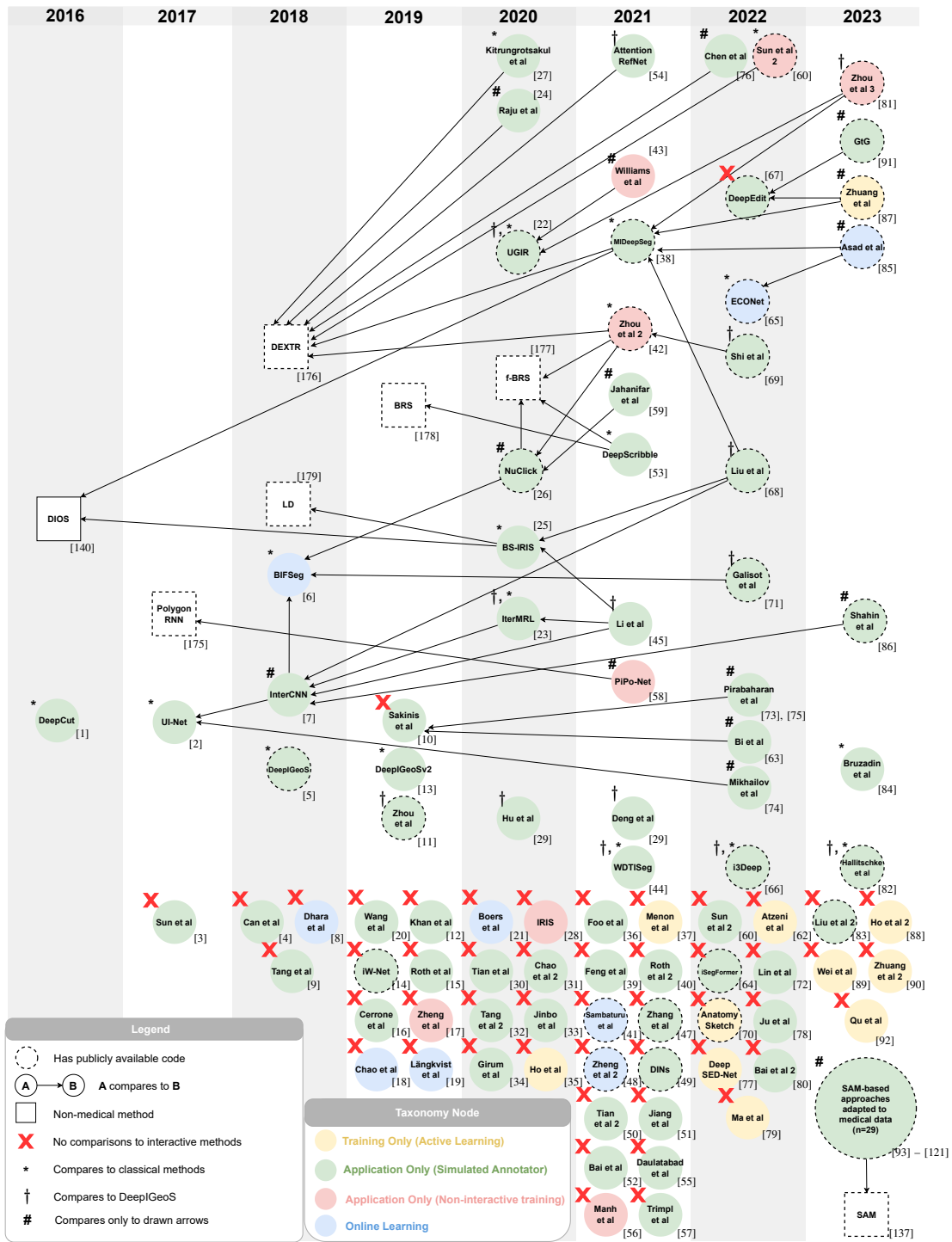


Fig. 6. Comparison graph of all the reviewed methods. Nodes are ordered temporally from left to right. Classical methods denote non-deep learning-based interactive methods before 2016. The star (*) and the dagger (†) are introduced to reduce the visual load in the figure caused by too many arrows.

weights. This openness and transparency in sharing resources are further bolstered by the presence of open-source projects like MONAI Label [149], AnatomySketch [70], RIL-Contour [150], BioMedisa [151], MITK [173], and PyMIC [174] which greatly facilitate the development and deployment of interactive deep medical models. Non-deep learning projects such as ilastik [168], ITK-Snap [169], and Li et al. [172], have also contributed to the open source development of interactive mod-

els and are widely used in the community. Additionally, this positive trajectory benefits from a growing reliance on openly available challenge datasets sourced from platforms such as Kaggle (www.kaggle.com), Grand Challenge (www.grand-challenge.org), and Synapse (www.synapse.org), promoting collaborative research and advancing the state of the art in the domain. All these tendencies are illustrated in Fig. 1. In our Appendixes, we provide links to code repositories of

all reviewed studies with publicly available code as well as links to all 185 public datasets used by the reviewed methods, streamlining access for future researchers.

D. Comparison Graph

Finally, we investigate the field’s practice of comparing proposed methods against relevant baselines. Since the scientific merit of a proposed method is measured as the gain over existing solutions, a comprehensive and up-to-date set of baseline methods is crucial for scientific progress in the field. Fig. 6 gives an overview over the comparison practices in deep interactive segmentation of medical images.

The most remarkable observation is the fact that a large fraction ($n=46$) of the 121 reviewed studies *do not compare against any prior work*. Another portion compares exclusively against “classical methods” ($n=6$), i.e. non-deep learning-based methods proposed before 2016, or exclusively against DeepI-GeoS [5] ($n=3$). Additionally, a large portion of studies ($n=37$) compare only to interactive methods which are not trained on medical data, such as DIOS [140], Polygon-RNN [175], DEXTR [176], Latent Diversity (LD) [179], BRS [178], f-BRS [177], and SAM [137]. Despite their shared characteristics, even methods from the same node of the presented taxonomy tree (see circle color in Fig. 6) are most often not compared against each other. Finally, the described acceleration of the field caused by the introduction of SAM seems to compromise the rigor of evaluation given that none of these approaches compares to methods other than the original non-medical SAM. This overall concerning status of a severe lack of cross-comparison in the field comes as a surprise given the positive trends towards reproducibility shown in Fig. 1.

VI. DISCUSSION AND FUTURE DIRECTIONS

Based on the key trends we have identified in Section V, we now derive and discuss the major challenges and opportunities for the field of deep interactive medical image segmentation. The discussion aims to provide a succinct summary of the field’s current trajectory while simultaneously identifying pivotal areas where course corrections are necessary.

A. Positive Trends

1) *Momentum in Research and Adaptation*: The increasing number of publications each year reflects significant momentum and rapid advancements in the field. Additionally, the fast adoption of new paradigms, such as SAM [137], exemplifies the field’s dynamic and responsive nature to emerging concepts and technologies.

2) *Enhanced Reproducibility and Open-Source Engagement*: There has been a notable surge in the use of open-source methods and public datasets. This trend not only facilitates more accessible development of customized models but also encourages the sharing of these models within the community. The proliferation of open-source frameworks specifically designed for interactive segmentation, like MONAI Label [149] and AnatomySketch [70], further underlines this commitment to reproducibility and collaborative growth.

B. Challenges and Opportunities

Our review highlights a pivotal challenge in the field: a discernible deficiency in scientific rigor in the evaluation of methods. These shortcomings are evident in various aspects, which we discuss in the following alongside opportunities to address them.

1) *Missing Baselines and Scattered Comparisons*: The absence of consistent baselines and scattered comparisons across studies is a major issue. Frequently, new methods are not compared with previous work, possibly due to a lack of awareness of other methods or no established evaluation protocols for interactive segmentation.

Opportunities: First, we hope that our taxonomy tree functions as a navigational tool, aiding researchers in categorizing their approaches and guiding them towards relevant existing methods. Second, the emergence of generalizing models like SAM [137] is a promising trend towards foundational baselines that allow for out-of-the-box comparisons under a uniform protocol. This approach can shift the field towards more structured and systematic improvements, similar to the effects of nnU-Net [136] in the realm of non-interactive medical segmentation, which, due to its out-of-the-box functionality, serves as a strong and standardized baseline in the field [146].

2) *No Standardized Benchmarking Datasets*: The lack of established benchmarking protocols across datasets and tasks in interactive medical image segmentation is a significant barrier. This gap impedes the objective evaluation and comparison of interactive models, which results in an inconsistent literature landscape with no definite state of the art.

Opportunities: The domain of non-medical interactive segmentation, particularly with natural images, has addressed this issue by leveraging extensively validated benchmark datasets like GrabCut [141], DAVIS [142], Pascal VOC [143], SBD [144], and Berkeley [145]. Moreover, these datasets are coupled with well-defined evaluation protocols and metrics, streamlining fair and systematic comparisons with previous research. A potential remedy for the fragmented nature of comparisons within the medical interactive segmentation field entails the establishment of a curated selection of the most exemplary datasets tailored to specific tasks and imaging modalities, complete with well-defined evaluation protocols. Such an approach would furnish researchers with a systematic framework for assessing their methodologies and documenting enhancements over prior methods.

3) *Lack of Adequate and Standardized Evaluation Metrics*: In the current landscape of deep interactive medical image segmentation, there are two significant challenges related to metric selection. The first prevalent issue is the over-reliance on a single metric for evaluating segmentation performance. As pointed out in [165], [170], this approach is too narrow and often fails to adequately capture the complexity and nuances of segmentation accuracy. Second, there is a conspicuous absence of user-centric metrics in evaluations. These metrics are essential to understand how effectively an interactive segmentation tool meets the practical needs and scenarios of its users, especially in the medical imaging context.

Opportunities: By adopting the comprehensive guidelines of “Metrics Reloaded” for metric selection, researchers can

ensure a more holistic evaluation of segmentation methods. This would involve using a diverse set of metrics that together provide a more complete picture of a method’s performance. In addition to technical metrics, emphasizing user-centric metrics in evaluations is crucial. This focus will shed light on the usability and practical effectiveness of interactive segmentation methods from the perspective of end-users, which is particularly important in clinical applications.

VII. CONCLUSION

In conclusion, our systematic review and the accompanying taxonomy tree stand as a pivotal resource for both researchers and practitioners within the field of deep interactive medical image segmentation. For researchers, this work simplifies the task of locating pertinent related studies, thereby enhancing the quality and relevance of their methodological proposals and evaluations. Practitioners, meanwhile, are empowered to swiftly identify and select methods that are optimally suited to their unique problem scenarios. Additionally, our review has not only identified key trends within the field but also thoroughly discussed the related challenges and opportunities for the future. Most importantly, we have pinpointed a concerning lack of scientific rigor in the evaluation of methods. This critical insight underlines the need for more standardized and systematic benchmarking practices in the field. Overall, we believe this work represents an important step towards implementing such standardized approaches, thereby fostering the development of more reliable, efficient, and effective solutions in deep interactive medical image segmentation.

APPENDIX A

CLICK GUIDANCE SIGNALS

Clicks are defined as 3D or 2D points, i.e., $c_i \in \mathbb{R}^3$ or $c_i \in \mathbb{R}^2$, depending on the dimensions of the input image. We define the set of clicks provided by the annotator as $\mathcal{C} := \{c_1, \dots, c_N\}$, where N is the number of clicks. Examples of click guidance signals are depicted in Fig. 7.

Disks. As disks and Gaussian heatmaps are computed independently for each click, they are defined for a single click c_i over voxels/pixels v in the image volume. Here, σ controls the radius of the disks in Eq. (1).

$$\text{disk}(v, c_i, \sigma) = \begin{cases} 1, & \text{if } \|v - c_i\|_2 \leq \sigma \\ 0, & \text{otherwise} \end{cases} \quad (1)$$

Gaussian Heatmaps apply Gaussian filters centered around each click c_i to create softer edges with an exponential decrease away from the click in Eq. (2).

$$\text{heatmap}(v, c_i, \sigma) = \exp\left(-\frac{\|v - c_i\|_2}{2\sigma^2}\right) \quad (2)$$

Euclidean Distance Transform (EDT) is defined in Eq. (3) as the minimum Euclidean distance between a voxel/pixel v and the set of clicks \mathcal{C} . It is similar to the disk signal in Eq. (1), but instead of filling the sphere with a constant value it computes the distance of each voxel to the closest click point.

$$\text{EDT}(v, \mathcal{C}) = \min_{c_i \in \mathcal{C}} \|v - c_i\|_2 \quad (3)$$

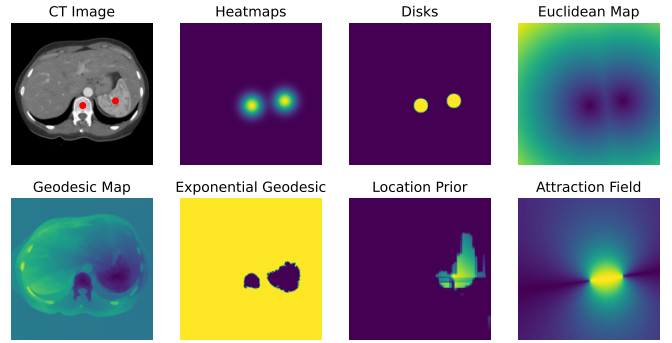


Fig. 7. Examples of click-based guidance signals.

Geodesic Distance Transform (GDT) is defined in Eq. (4) as the shortest geodesic path distance between each voxel in the volume and the closest click in the set \mathcal{C} [181]. The shortest geodesic path in GDT also takes into account intensity differences between voxels along the path. The shortest path is denoted as Φ in Eq. (4) and can be computed with, e.g., the Fast Marching method [182].

$$\text{GDT}(v, \mathcal{C}) = \min_{c_i \in \mathcal{C}} \Phi(v, c_i) \quad (4)$$

Exponentialized Geodesic distance (exp-GDT) proposed in MIDeepSeg [38] is defined in Eq. (5) as an exponentiation of GDT from Eq. (4):

$$\text{exp-GDT}(v, \mathcal{C}) = 1 - \exp(-\text{GDT}(v, \mathcal{C})) \quad (5)$$

Location Prior (LP), as proposed by Sun et al. [3], incorporates both the Manhattan distance and the information about crossed edges detected by a Canny edge detector [123]. The LP assigns an initial intensity value of 255 to the center voxel, denoted as $c = (c_x, c_y)$, and decreases this value by 1 for each vertical or horizontal step taken. Furthermore, when a step crosses a detected edge the intensity value decreases by an additional 10. LP combines the notion of distance with the presence of edges to provide a comprehensive measure for location estimation.

$$\text{LP}(v) = \left(0, 255 - \sum_{i=c_x}^{v_x} \sum_{j=c_y}^{v_y} \begin{cases} -10 & \text{if Canny}(I)(x_i, y_i) == 1 \text{ and edge_crossed} \\ -1 & \text{otherwise} \end{cases} \right)$$

Attraction Field Weight Map (AF), as introduced in [14], draws inspiration from the attraction field generated by punctual electric charges of opposite values. AF utilizes unitary gradient fields, denoted as $\nabla S_i(v)$, which are centered around two clicks, namely c_1 and c_2 . These gradient fields exhibit higher values between the clicks, indicating their significance for the segmentation process. The hyperparameter $p \in \mathbb{R}$ controls the decay of the vectors’ magnitude.

$$\text{AF}(v, c_1, c_2) = \frac{\nabla S_1(v)}{|\nabla S_1(v)|^p} - \frac{\nabla S_2(v)}{|\nabla S_2(v)|^p} \quad (6)$$

$$\nabla S_i(v) = \frac{2(v_x - c_{ix}) + 2(v_y - c_{iy}) + (v_z - c_{iz})}{2\|v - c_i\|} \quad (7)$$

APPENDIX B SCRIBBLE GUIDANCE SIGNALS

Scribbles are defined as 3D or 2D sets of points \mathcal{C} , i.e., $\mathcal{C} := \{c_1, \dots, c_N\}$, where $c_i \in \mathbb{R}^3$ or $c_i \in \mathbb{R}^2$, depending on the dimensions of the input image. In a formal sense, scribbles can be seen as a set of clicks. However, conceptually, scribbles manifest as a diverse array of interactions, encompassing structured actions like deliberate line strokes, spontaneous unstructured marks such as random dabs, or a fusion of both. Examples of scribble guidance signals are shown in Fig. 8.

Gaussian Heatmaps for scribbles are derived from the click heatmaps in Eq. (2) by summing all click heatmaps into one guidance signal, resulting in Eq. (8).

$$\text{heatmap}(v, \mathcal{C}, \sigma) = \sum_{i=0}^N \text{heatmap}(v, c_i, \sigma) \quad (8)$$

The **Euclidean Distance Transform** (EDT) and the **Geodesic Distance Transform** (GDT) do not differ in any way from their click-based versions in Eq. (3) and (4) since those are already defined over a set of points \mathcal{C} .

Subset of Ground-Truth. One way to simulate scribbles with a robot user is to randomly sample a subset of the ground-truth mask \mathcal{M} . As scribbles do not inherently adhere to a specific structure, this typically manifests as a series of random clicks, resembling the illustration in Fig. 8.

$$\mathcal{C} = \{c_i\}_{i=1}^N, \text{ where } x_i \sim \mathcal{M} \text{ and } N \leq |\mathcal{M}| \quad (9)$$

Ground-truth Skeletonization is another way to simulate scribbles with a robot user by representing the morphological structure of the ground-truth mask \mathcal{M} in the scribble \mathcal{C} . The skeleton(\cdot) in Eq. (10) consists of the 1-pixel wide medial axes of the mask [184]. An example is depicted in Fig. 8.

$$\mathcal{C} = \text{skeleton}(\mathcal{M}) \quad (10)$$

Error Skeletonization is a way to simulate iterative scribbles, which are used to correct the previous prediction with a corrective stroke [27], [33], [53], [54]. The scribbles are computed the same way as in Eq. (10) but over the missegmented region \mathcal{E} instead of the ground-truth mask \mathcal{M} .

$$\mathcal{C} = \text{skeleton}(\mathcal{E}) \quad (11)$$

Ground-truth Scribbles are a guidance signal where the raw scribble set \mathcal{C} provided by a real human annotator is used directly as a representation of the interaction. This is often done to avoid information leaking into neighboring voxels, e.g., through applying a distance transform or a heatmap to the scribbles [75], [91].

APPENDIX C IMPLICIT SIGNALS AND OTHER GUIDANCE SIGNALS

Implicit signals subtly incorporate interactions into the model’s training or inference, without using structured inputs like spherical heatmaps or skeletonized scribbles. Examples include weights in the loss function based on the distance

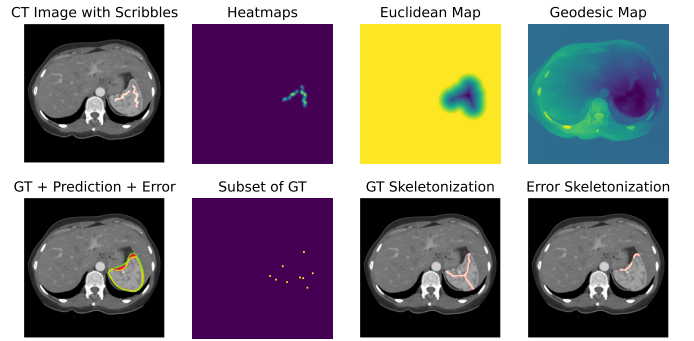


Fig. 8. Examples of scribble-based guidance signals. GT: Ground-truth mask. Bottom left image – green: GT, yellow: model prediction, red: error.

to clicks/scribbles, or cropping inputs via bounding box interactions to selectively feed to the model. Implicit signals are represented by an *action*, such as loss function *weighting*, or input *cropping*. In contrast, explicit signals are conveyed through a defined *structure*, like Gaussian *heatmaps* or error *skeletons*.

Less common guidance signals encompass vertex polygons and B-splines, employed to outline the segmentation mask boundary [50], [70]. Users can adjust the boundary by manipulating vertices or control points of the spline. Another signal involves leveraging predictions from an auxiliary approach, such as GraphCut [131], which generates pseudolabels added to the input image. Additionally, methods utilizing the Segment Anything Model (SAM) [137] use positional encodings to represent bounding box or click coordinates.

APPENDIX D PUBLIC DATASETS AND PUBLIC CODE LINKS

APPENDIX E FULL LIST OF LITERATURE DATABASES AND VENUES IN OUR SEARCH STRATEGY

APPENDIX F PRISMA 2020 CHECKLIST

Tables VIII, IX, and X show the Preferred Reporting Items for Systematic Reviews and Meta-Analyses (PRISMA) 2020 [139] checklist and where we have reported each item in our review. Certain items are marked with “-” since they either do not apply to our review or are excluded due to the technical nature of our study, which diverges from the clinical emphasis of the PRISMA guidelines.

While our review predominantly centers on technical methodology rather than clinical outcomes, we make an effort to adhere to the definition of “synthesis methods” within the PRISMA guidelines as closely as possible. In this review, we define synthesis methods as the systematic analysis and summarization of results from the reviewed studies to draw comprehensive conclusions and identify overarching patterns and trends. Our review’s synthesis methods (rows 13a-13f in Table VIII) encompass the following elements:

- Tabular representation of all studies: A structured arrangement of studies and their corresponding data items in a clear and accessible format. This information is

TABLE III
PUBLIC DATASETS USED FOR INTERACTIVE SEGMENTATION

Table with 4 columns: Abbreviation, Dataset, Link, Modality. Lists various medical datasets like ACDC, BraTS15, etc.

TABLE V
LIST OF ALL LITERATURE DATABASES USED IN STEP 1 OF OUR SYSTEMATIC SEARCH

Table with 2 columns: Literature Database, Link. Lists databases like Google Scholar, PubMed, etc.

TABLE VI
LIST OF ALL CONFERENCES, JOURNALS, AND CONFERENCE WORKSHOPS USED IN STEP 4 OF OUR SYSTEMATIC SEARCH.

Table with 4 columns: Venue, Abbreviation, Type, Link. Lists conferences like Applied Sciences, Artificial Intelligence in Medicine, etc.

TABLE IV
LIST OF ALL REVIEWED INTERACTIVE METHODS WITH PUBLICLY AVAILABLE CODE

Table with 2 columns: Paper, Code. Lists papers like DeepGeoS [5], Zhou et al. [11], etc.

TABLE VII
RETRIEVED STUDIES FOR EACH KEYWORD COMBINATION

Table with 5 columns: Keywords, Interactive Segmentation, Interactive Delineation, Human-in-the-Loop Segmentation, Human-in-the-Loop Delineation. Shows counts for different search combinations.

presented in Table I and Table II, located on pages 4 and 5, respectively.
• Introduction of a taxonomy: A taxonomy tree, introduced

in Section III, paragraphs 1-3, to offer a structured categorization of the reviewed studies.
• Visual rationale for study categorization: We utilize Fig. 4 to visually illustrate the rationale guiding the categorization within the taxonomy tree, ensuring transparency

throughout the categorization process.

- Visualization and analysis of the data items of the reviewed studies: We analyze the distribution of data items to unveil patterns, visually presented in Fig. 5, and provide a comprehensive discussion of potential reasons for these patterns in Section V-A.
- Analysis of the cross-comparisons: We analyze the comparisons between reviewed studies in Fig. 7, and explore the underlying reasons for the absence of systematic comparisons within the field in Section V-D.

REFERENCES

- [1] M. Rajchl, M. C. Lee, O. Oktay, K. Kamnitsas, J. Passerat-Palmbach, W. Bai, M. Damodaram, M. A. Rutherford, J. V. Hajnal, B. Kainz, et al., “Deepcut: Object segmentation from bounding box annotations using convolutional neural networks,” *IEEE transactions on medical imaging*, vol. 36, no. 2, pp. 674–683, 2016.
- [2] M. Amrehn, S. Gaube, M. Unberath, F. Schebesch, T. Horz, M. Strumia, S. Steidl, M. Kowarschik, and A. Maier, “Ui-net: interactive artificial neural networks for iterative image segmentation based on a user model,” in *Proceedings of the Eurographics Workshop on Visual Computing for Biology and Medicine*, pp. 143–147, 2017.
- [3] J. Sun, Y. Shi, Y. Gao, and D. Shen, “A point says a lot: an interactive segmentation method for mr prostate via one-point labeling,” in *Machine Learning in Medical Imaging: 8th International Workshop, MLMI 2017, Held in Conjunction with MICCAI 2017, Quebec City, QC, Canada, September 10, 2017, Proceedings 8*, pp. 220–228, Springer, 2017.
- [4] Y. B. Can, K. Chaitanya, B. Mustafa, L. M. Koch, E. Konukoglu, and C. F. Baumgartner, “Learning to segment medical images with scribble-supervision alone,” in *Deep Learning in Medical Image Analysis and Multimodal Learning for Clinical Decision Support: 4th International Workshop, DLMIA 2018, and 8th International Workshop, ML-CDS 2018, Held in Conjunction with MICCAI 2018, Granada, Spain, September 20, 2018, Proceedings 4*, pp. 236–244, Springer, 2018.
- [5] G. Wang, M. A. Zuluaga, W. Li, R. Pratt, P. A. Patel, M. Aertsen, T. Doel, A. L. David, J. Deprest, S. Ourselin, et al., “Deepigeos: a deep interactive geodesic framework for medical image segmentation,” *IEEE transactions on pattern analysis and machine intelligence*, vol. 41, no. 7, pp. 1559–1572, 2018.
- [6] G. Wang, W. Li, M. A. Zuluaga, R. Pratt, P. A. Patel, M. Aertsen, T. Doel, A. L. David, J. Deprest, S. Ourselin, et al., “Interactive medical image segmentation using deep learning with image-specific fine tuning,” *IEEE transactions on medical imaging*, vol. 37, no. 7, pp. 1562–1573, 2018.
- [7] G. Bredell, C. Tanner, and E. Konukoglu, “Iterative interaction training for segmentation editing networks,” in *Machine Learning in Medical Imaging: 9th International Workshop, MLMI 2018, Held in Conjunction with MICCAI 2018, Granada, Spain, September 16, 2018, Proceedings 9*, pp. 363–370, Springer, 2018.
- [8] A. K. Dhara, K. R. Ayyalasomayajula, E. Arvids, M. Fahlström, J. Wikström, E.-M. Larsson, and R. Strand, “Segmentation of post-operative glioblastoma in mri by u-net with patient-specific interactive refinement,” in *Brainlesion: Glioma, Multiple Sclerosis, Stroke and Traumatic Brain Injuries: 4th International Workshop, BrainLes 2018, Held in Conjunction with MICCAI 2018, Granada, Spain, September 16, 2018, Revised Selected Papers, Part I 4*, pp. 115–122, Springer, 2019.
- [9] Y. Tang, A. P. Harrison, M. Bagheri, J. Xiao, and R. M. Summers, “Semi-automatic recist labeling on ct scans with cascaded convolutional neural networks,” in *Medical Image Computing and Computer Assisted Intervention–MICCAI 2018: 21st International Conference, Granada, Spain, September 16–20, 2018, Proceedings, Part IV 11*, pp. 405–413, Springer, 2018.
- [10] T. Sakinis, F. Milletari, H. Roth, P. Korfiatis, P. Kostandy, K. Philbrick, Z. Akkus, Z. Xu, D. Xu, and B. J. Erickson, “Interactive segmentation of medical images through fully convolutional neural networks,” *arXiv preprint arXiv:1903.08205*, 2019.
- [11] B. Zhou, L. Chen, and Z. Wang, “Interactive deep editing framework for medical image segmentation,” in *Medical Image Computing and Computer Assisted Intervention–MICCAI 2019: 22nd International Conference, Shenzhen, China, October 13–17, 2019, Proceedings, Part III 22*, pp. 329–337, Springer, 2019.
- [12] S. Khan, A. H. Shahin, J. Villafruela, J. Shen, and L. Shao, “Extreme points derived confidence map as a cue for class-agnostic interactive segmentation using deep neural network,” in *Medical Image Computing and Computer Assisted Intervention–MICCAI 2019: 22nd International Conference, Shenzhen, China, October 13–17, 2019, Proceedings, Part II 22*, pp. 66–73, Springer, 2019.
- [13] W. Lei, H. Wang, R. Gu, S. Zhang, S. Zhang, and G. Wang, “Deepigeos-v2: deep interactive segmentation of multiple organs from head and neck images with lightweight cnns,” in *Large-Scale Annotation of Biomedical Data and Expert Label Synthesis and Hardware Aware Learning for Medical Imaging and Computer Assisted Intervention: International Workshops, LABELS 2019, HAL-MICCAI 2019, and CuRIOUS 2019, Held in Conjunction with MICCAI 2019, Shenzhen, China, October 13 and 17, 2019, Proceedings 4*, pp. 61–69, Springer, 2019.
- [14] G. Aresta, C. Jacobs, T. Araújo, A. Cunha, I. Ramos, B. van Ginneken, and A. Campilho, “iw-net: an automatic and minimalistic interactive lung nodule segmentation deep network,” *Scientific reports*, vol. 9, no. 1, pp. 1–9, 2019.
- [15] H. Roth, L. Zhang, D. Yang, F. Milletari, Z. Xu, X. Wang, and D. Xu, “Weakly supervised segmentation from extreme points,” in *Large-Scale Annotation of Biomedical Data and Expert Label Synthesis and Hardware Aware Learning for Medical Imaging and Computer Assisted Intervention: International Workshops, LABELS 2019, HAL-MICCAI 2019, and CuRIOUS 2019, Held in Conjunction with MICCAI 2019, Shenzhen, China, October 13 and 17, 2019, Proceedings 4*, pp. 42–50, Springer, 2019.
- [16] L. Cerrone, A. Zeilmann, and F. A. Hamprecht, “End-to-end learned random walker for seeded image segmentation,” in *Proceedings of the IEEE/CVF Conference on Computer Vision and Pattern Recognition*, pp. 12559–12568, 2019.
- [17] H. Zheng, Y. Chen, X. Yue, and C. Ma, “Deep interactive segmentation of uncertain regions with shadowed sets,” in *Proceedings of the Third International Symposium on Image Computing and Digital Medicine*, pp. 244–248, 2019.
- [18] C.-H. Chao, Y.-C. Cheng, H.-T. Cheng, C.-W. Huang, T.-Y. Ho, C.-K. Tseng, L. Lu, and M. Sun, “Radiotherapy target contouring with convolutional gated graph neural network,” *arXiv preprint arXiv:1904.03086*, 2019.
- [19] M. Långkvist, J. Widell, P. Thunberg, A. Loutfi, and M. Lidén, “Interactive user interface based on convolutional auto-encoders for annotating ct-scans,” *arXiv preprint arXiv:1904.11701*, 2019.
- [20] X. Wang, L. Zhang, H. Roth, D. Xu, and Z. Xu, “Interactive 3d segmentation editing and refinement via gated graph neural networks,” in *Graph Learning in Medical Imaging: First International Workshop, GLMI 2019, Held in Conjunction with MICCAI 2019, Shenzhen, China, October 17, 2019, Proceedings*, pp. 9–17, Springer, 2019.
- [21] T. Boers, Y. Hu, E. Gibson, D. Barratt, E. Bonmati, J. Krdzalic, F. van der Heijden, J. Hermans, and H. Huisman, “Interactive 3d u-net for the segmentation of the pancreas in computed tomography scans,” *Physics in Medicine & Biology*, vol. 65, no. 6, p. 065002, 2020.
- [22] G. Wang, M. Aertsen, J. Deprest, S. Ourselin, T. Vercauteren, and S. Zhang, “Uncertainty-guided efficient interactive refinement of fetal brain segmentation from stacks of mri slices,” in *Medical Image Computing and Computer Assisted Intervention–MICCAI 2020: 23rd International Conference, Lima, Peru, October 4–8, 2020, Proceedings, Part IV 23*, pp. 279–288, Springer, 2020.
- [23] X. Liao, W. Li, Q. Xu, X. Wang, B. Jin, X. Zhang, Y. Wang, and Y. Zhang, “Iteratively-refined interactive 3d medical image segmentation with multi-agent reinforcement learning,” in *Proceedings of the IEEE/CVF conference on computer vision and pattern recognition*, pp. 9394–9402, 2020.
- [24] A. Raju, Z. Ji, C. T. Cheng, J. Cai, J. Huang, J. Xiao, L. Lu, C. Liao, and A. P. Harrison, “User-guided domain adaptation for rapid annotation from user interactions: a study on pathological liver segmentation,” in *Medical Image Computing and Computer Assisted Intervention–MICCAI 2020: 23rd International Conference, Lima, Peru, October 4–8, 2020, Proceedings, Part I*, pp. 457–467, Springer, 2020.
- [25] C. Ma, Q. Xu, X. Wang, B. Jin, X. Zhang, Y. Wang, and Y. Zhang, “Boundary-aware supervoxel-level iteratively refined interactive 3d image segmentation with multi-agent reinforcement learning,” *IEEE Transactions on Medical Imaging*, vol. 40, no. 10, pp. 2563–2574, 2020.
- [26] N. A. Koohbanani, M. Jahanifar, N. Z. Tajadin, and N. Rajpoot, “Nuclick: a deep learning framework for interactive segmentation of microscopic images,” *Medical Image Analysis*, vol. 65, p. 101771, 2020.

TABLE VIII
PRISMA 2020 CHECKLIST

Section and Topic	Item	Checklist Item	Location where item is reported
TITLE			
Title	1	Identify the report as a systematic review.	Title
ABSTRACT			
Abstract	2	See the PRISMA 2020 for Abstracts Checklist.	Appendix F, Table X
INTRODUCTION			
Rationale	3	Describe the rationale for the review in the context of existing knowledge.	Page 1, Section I, paragraph 4
Objectives	4	Provide an explicit statement of the objective(s) or question(s) the review addresses.	Page 1, Section I, paragraph 5 (bulleted list)
METHODS			
Eligibility Criteria	5	Specify the inclusion and exclusion criteria for the review and how studies were grouped for the syntheses	Page 3, Section III, paragraph 1
Information sources	6	Specify all databases, registers, websites, organizations, reference lists, and other sources searched or consulted to identify studies. Specify the date when each source was last searched or consulted.	Page 2, Section III, paragraph 1
Search strategy	7	Present the full search strategies for all databases, registers, and websites, including any filters and limits used.	Page 2, Section III, paragraph 1; and page 3, Section III, paragraphs 1 and 3
Selection process	8	Specify the methods used to decide whether a study met the inclusion criteria of the review, including how many reviewers screened each record and each report retrieved, and whether they worked independently.	Page 3, Section III, paragraph 2
Data collection process	9	Specify the methods used to collect data from reports, including how many reviewers collected data from each report, whether they worked independently, and any processes for obtaining or confirming data from study investigators.	Page 3, Section III, paragraph 4
Data items	10a	List and define all outcomes for which data were sought. Specify whether all results that were compatible with each outcome domain in each study were sought (e.g. for all measures, time points, analyses), and if not, the methods used to decide which results to collect.	Page 3, Section III, paragraph 4
	10b	List and define all other variables for which data were sought (e.g. participant and intervention characteristics, funding sources). Describe any assumptions made about any missing or unclear information.	Page 3, Section III, paragraph 4
Study risk of bias assessment	11	Specify the methods used to assess the risk of bias in the included studies, including details of the tool(s) used, how many reviewers assessed each study, and whether they worked independently.	-
Effect measures	12	Specify for each outcome the effect measure(s) (e.g. risk ratio, mean difference) used in the synthesis or presentation of results	-
Synthesis methods	13a	Describe the processes used to decide which studies were eligible for each synthesis (e.g. tabulating the study intervention characteristics and comparing against the planned groups for each synthesis (item #5)).	Page 3, Section IV, paragraphs 1-3; page 6, Fig. 3; and page 7, Fig. 4
	13b	Describe any methods required to prepare the data for presentation or synthesis, such as handling of missing summary statistics, or data conversions.	Page 3, Section IV, paragraphs 1-3
	13c	Describe any methods used to tabulate or visually display results of individual studies and syntheses.	Page 3, paragraphs 1-3; page 4, Table I; and page 5, Table II
	13d	Describe any methods used to synthesize results and provide a rationale for the choice(s).	Page 3, Section IV, paragraphs 1-3; and page 7, Fig. 7
	13e	Describe any methods used to explore possible causes of heterogeneity among study results (e.g. subgroup analysis, meta-regression).	Page 15, Section V-D; and page 6, Fig. 6
	13f	Describe any sensitivity analyses conducted to assess the robustness of the synthesized results.	-
Reporting bias assessment	14	Describe any methods used to assess the risk of bias due to missing results in a synthesis (arising from reporting biases).	-
Certainty assessment	15	Describe any methods used to assess certainty (or confidence) in the body of evidence for an outcome.	-

TABLE IX
PRISMA 2020 CHECKLIST, CONTINUED

Section and Topic	Item	Checklist Item	Location where item is reported
RESULTS			
Study selection	16a	Describe the results of the search and selection process, from the number of records identified in the search to the number of studies included in the review, ideally using a flow diagram.	Page 2, Fig. 2; page 3, paragraph 3; and Appendix F, Table VII
	16b	Cite studies that might appear to meet the inclusion criteria, but which were excluded, and explain why they were excluded.	Page 3, Section III, paragraph 5
Study Characteristics	17	Cite each included study and present its characteristics.	Pages 3-12, Sections IV-A, IV-B, and IV-C (all paragraphs each) cite and describe all studies in detail; page 4, Table I; page 5, Table II; and page 14, Fig. 6 contains citations to all studies
Risk of bias in studies	18	Present assessments of risk of bias for each included study.	-
Results of individual studies	19	For all outcomes, present, for each study: (a) summary statistics for each group (where appropriate) and (b) an effect estimate and its precision (e.g. confidence/credible interval), ideally using structured tables or plots.	-
Results of syntheses	20a	For each synthesis, briefly summarise the characteristics and risk of bias among contributing studies	-
	20b	Present results of all statistical syntheses conducted.	Pages 12-13, Section V-A (all paragraphs); and page 13 Fig. 5
	20c	Present results of all investigations of possible causes of heterogeneity among study results.	-
	20d	Present results of all sensitivity analyses conducted to assess the robustness of the synthesized results.	-
Reporting biases	21	Present assessments of risk of bias due to missing results (arising from reporting biases) for each synthesis assessed.	-
Certainty of evidence	22	Present assessments of certainty (or confidence) in the body of evidence for each outcome assessed.	-
DISCUSSION			
Discussion	23a	Provide a general interpretation of the results in the context of other evidence.	Page 15, Section VI, paragraph 1
	23b	Discuss any limitations of the evidence included in the review.	-
	23c	Discuss any limitations of the review processes used.	-
	23d	Discuss implications of the results for practice, policy, and future research.	Page 15, Section IV-B (all paragraphs)
OTHER INFORMATION			
Registration and protocol	24a	Provide registration information for the review, including register name and registration number, or state that the review was not registered.	The review was not registered
	24b	Indicate where the review protocol can be accessed, or state that a protocol was not prepared.	A protocol was not provided
	24c	Describe and explain any amendments to the information provided at registration or in the protocol.	A protocol was not provided
Support	25	Describe sources of financial or non-financial support for the review, and the role of the funders or sponsors in the review.	-
Competing interests	26	Declare any competing interests of review authors.	-
Availability of data, code and other materials	27	Report which of the following are publicly available and where they can be found: template data collection forms; data extracted from included studies; data used for all analyses; analytic code; any other materials used in the review.	-

TABLE X
PRISMA 2020 ABSTRACT CHECKLIST

Section and Topic	Item	Checklist Item	Reported (Yes/No)
TITLE			
Title	1	Identify the report as a systematic review.	Yes
BACKGROUND			
Objectives	2	Provide an explicit statement of the main objective(s) or question(s) the review addresses.	Yes
METHODS			
Eligibility criteria	3	Specify the inclusion and exclusion criteria for the review.	No
Information sources	4	Specify the information sources (e.g. databases, registers) used to identify studies and the date when each was last searched.	No
Risk of bias	5	Specify the methods used to assess risk of bias in the included studies.	No
Synthesis of results	6	Specify the methods used to present and synthesize results.	Yes
RESULTS			
Included studies	7	Give the total number of included studies and participants and summarize relevant characteristics of studies.	Yes
Synthesis of results	8	Present results for main outcomes, preferably indicating the number of included studies and participants for each. If meta-analysis was done, report the summary estimate and confidence/credible interval.	No
DISCUSSION			
Limitations of evidence	9	Provide a brief summary of the limitations of the evidence included in the review (e.g. study risk of bias, inconsistency, and imprecision).	No
Interpretation	10	Provide a general interpretation of the results and important implications.	Yes
OTHER			
Funding	11	Specify the primary source of funding for the review.	No
Registration	12	Provide the register name and registration number.	No

- [27] T. Kitrungrotsakul, I. Yutaro, L. Lin, R. Tong, J. Li, and Y.-W. Chen, "Interactive deep refinement network for medical image segmentation," *arXiv preprint arXiv:2006.15320*, 2020.
- [28] A. Pepe, R. Schussnig, J. Li, C. Gsaxner, X. Chen, T.-P. Fries, and J. Egger, "Iris: interactive real-time feedback image segmentation with deep learning," in *Medical Imaging 2020: Biomedical Applications in Molecular, Structural, and Functional Imaging*, vol. 11317, pp. 181–186, SPIE, 2020.
- [29] W. Hu, X. Yao, Z. Zheng, X. Zhang, Y. Zhong, X. Wang, Y. Zhang, and Y. Wang, "Error attention interactive segmentation of medical image through matting and fusion," in *Machine Learning in Medical Imaging: 11th International Workshop, MLMI 2020, Held in Conjunction with MICCAI 2020, Lima, Peru, October 4, 2020, Proceedings 11*, pp. 11–20, Springer, 2020.
- [30] Z. Tian, X. Li, Y. Zheng, Z. Chen, Z. Shi, L. Liu, and B. Fei, "Graph-convolutional-network-based interactive prostate segmentation in mr images," *Medical physics*, vol. 47, no. 9, pp. 4164–4176, 2020.
- [31] C.-H. Chao, H.-T. Cheng, T.-Y. Ho, L. Lu, and M. Sun, "Interactive radiotherapy target delineation with 3d-fused context propagation," *arXiv preprint arXiv:2012.06873*, 2020.
- [32] Y. Tang, K. Yan, J. Xiao, and R. M. Summers, "One click lesion recist measurement and segmentation on ct scans," in *Medical Image Computing and Computer Assisted Intervention–MICCAI 2020: 23rd International Conference, Lima, Peru, October 4–8, 2020, Proceedings, Part IV 23*, pp. 573–583, Springer, 2020.
- [33] H. Jinbo, T. Kitrungrotsaku, Y. Iwamoto, L. Lin, H. Hu, and Y.-W. Chen, "Development of an interactive semantic medical image segmentation system," in *2020 IEEE 9th Global Conference on Consumer Electronics (GCCE)*, pp. 678–681, IEEE, 2020.
- [34] K. B. Girum, G. Créhange, R. Hussain, and A. Lalande, "Fast interactive medical image segmentation with weakly supervised deep learning method," *International Journal of Computer Assisted Radiology and Surgery*, vol. 15, pp. 1437–1444, 2020.
- [35] D. J. Ho, N. P. Agaram, P. J. Schüffler, C. M. Vanderbilt, M.-H. Jean, M. R. Hameed, and T. J. Fuchs, "Deep interactive learning: an efficient labeling approach for deep learning-based osteosarcoma treatment response assessment," in *Medical Image Computing and Computer Assisted Intervention–MICCAI 2020: 23rd International Conference, Lima, Peru, October 4–8, 2020, Proceedings, Part V 23*, pp. 540–549, Springer, 2020.
- [36] M. X.-L. Foo, S. T. Kim, M. Paschali, L. Goli, E. Burian, M. Makowski, R. Braren, N. Navab, and T. Wendler, "Interactive segmentation for covid-19 infection quantification on longitudinal ct scans," *arXiv preprint arXiv:2110.00948*, 2021.
- [37] A. Menon, P. Singh, P. Vinod, and C. Jawahar, "Interactive learning for assisting whole slide image annotation," in *Asian Conference on Pattern Recognition*, pp. 504–517, Springer, 2021.
- [38] X. Luo, G. Wang, T. Song, J. Zhang, M. Aertsen, J. Deprest, S. Ourselin, T. Vercauteren, and S. Zhang, "Mideepseg: Minimally interactive segmentation of unseen objects from medical images using deep learning," *Medical image analysis*, vol. 72, p. 102102, 2021.
- [39] R. Feng, X. Zheng, T. Gao, J. Chen, W. Wang, D. Z. Chen, and J. Wu, "Interactive few-shot learning: Limited supervision, better medical image segmentation," *IEEE Transactions on Medical Imaging*, vol. 40, no. 10, pp. 2575–2588, 2021.
- [40] H. R. Roth, D. Yang, Z. Xu, X. Wang, and D. Xu, "Going to extremes: weakly supervised medical image segmentation," *Machine Learning and Knowledge Extraction*, vol. 3, no. 2, pp. 507–524, 2021.
- [41] B. Sambaturu, A. Gupta, C. Jawahar, and C. Arora, "Efficient and generic interactive segmentation framework to correct mispredictions during clinical evaluation of medical images," in *Medical Image Computing and Computer Assisted Intervention–MICCAI 2021: 24th International Conference, Strasbourg, France, September 27–October 1, 2021, Proceedings, Part II 24*, pp. 625–635, Springer, 2021.
- [42] T. Zhou, L. Li, G. Bredell, J. Li, and E. Konukoglu, "Quality-aware memory network for interactive volumetric image segmentation," in *Medical Image Computing and Computer Assisted Intervention–MICCAI 2021: 24th International Conference, Strasbourg, France, September 27–October 1, 2021, Proceedings, Part II 24*, pp. 560–570, Springer, 2021.
- [43] H. Williams, J. Pedrosa, L. Cattani, S. Housmans, T. Vercauteren, J. Deprest, and J. D'hooge, "Interactive segmentation via deep learning and b-spline explicit active surfaces," in *Medical Image Computing and Computer Assisted Intervention–MICCAI 2021: 24th International Conference, Strasbourg, France, September 27–October 1, 2021, Proceedings, Part I 24*, pp. 315–325, Springer, 2021.
- [44] X. Li, M. Qiao, Y. Guo, J. Zhou, S. Zhou, C. Chang, and Y. Wang, "Wdtiseg: One-stage interactive segmentation for breast ultrasound

- image using weighted distance transform and shape-aware compound loss." *Applied Sciences*, vol. 11, no. 14, p. 6279, 2021.
- [45] W. Li, Q. Xu, C. Shen, B. Hu, F. Zhu, Y. Li, B. Jin, and X. Wang, "Interactive medical image segmentation with self-adaptive confidence calibration," *arXiv preprint arXiv:2111.07716*, 2021.
- [46] J. Deng and X. Xie, "3d interactive segmentation with semi-implicit representation and active learning," *IEEE Transactions on Image Processing*, vol. 30, pp. 9402–9417, 2021.
- [47] J. Zhang, Y. Shi, J. Sun, L. Wang, L. Zhou, Y. Gao, and D. Shen, "Interactive medical image segmentation via a point-based interaction," *Artificial Intelligence in Medicine*, vol. 111, p. 101998, 2021.
- [48] E. Zheng, Q. Yu, R. Li, P. Shi, and A. Haake, "A continual learning framework for uncertainty-aware interactive image segmentation," in *Proceedings of the AAAI Conference on Artificial Intelligence*, vol. 35, pp. 6030–6038, 2021.
- [49] J.-W. Zhang, W. Chen, K. I. Ly, X. Zhang, F. Yan, J. Jordan, G. Harris, S. Plotkin, P. Hao, and W. Cai, "Dins: deep interactive networks for neurofibroma segmentation in neurofibromatosis type 1 on whole-body mri," *IEEE Journal of Biomedical and Health Informatics*, vol. 26, no. 2, pp. 786–797, 2021.
- [50] Z. Tian, X. Li, Z. Chen, Y. Zheng, H. Fan, Z. Li, C. Li, and S. Du, "Interactive prostate mr image segmentation based on convlstm and ggnn," *Neurocomputing*, vol. 438, pp. 84–93, 2021.
- [51] D. Jiang, Y. Wang, F. Zhou, H. Ma, W. Zhang, W. Fang, P. Zhao, and Z. Tong, "Residual refinement for interactive skin lesion segmentation," *Journal of Biomedical Semantics*, vol. 12, no. 1, p. 22, 2021.
- [52] Y. Bai, G. Sun, Y. Li, L. Shen, and L. Zhang, "Progressive medical image annotation with convolutional neural network-based interactive segmentation method," in *Medical Imaging 2021: Image Processing*, vol. 11596, pp. 732–742, SPIE, 2021.
- [53] S. Cho, H. Jang, J. W. Tan, and W.-K. Jeong, "Deepscribble: interactive pathology image segmentation using deep neural networks with scribbles," in *2021 IEEE 18th International Symposium on Biomedical Imaging (ISBI)*, pp. 761–765, IEEE, 2021.
- [54] T. Kitrungratsakul, Q. Chen, H. Wu, Y. Iwamoto, H. Hu, W. Zhu, C. Chen, F. Xu, Y. Zhou, L. Lin, *et al.*, "Attention-refnet: Interactive attention refinement network for infected area segmentation of covid-19," *IEEE Journal of Biomedical and Health Informatics*, vol. 25, no. 7, pp. 2363–2373, 2021.
- [55] R. Daulatabad, R. Vega, J. L. Jaremkov, J. Kapur, A. R. Hareendranathan, and K. Punithakumar, "Integrating user-input into deep convolutional neural networks for thyroid nodule segmentation," in *2021 43rd Annual International Conference of the IEEE Engineering in Medicine & Biology Society (EMBC)*, pp. 2637–2640, IEEE, 2021.
- [56] X. H. Manh, H. Vu, X. D. Nguyen, L. H. P. Tu, H. D. Viet, P. B. Nguyen, and M. H. Nguyen, "Interactive z-line segmentation tool for upper gastrointestinal endoscopy images using binary partition tree and u-net," in *2021 RIVF International Conference on Computing and Communication Technologies (RIVF)*, pp. 1–6, IEEE, 2021.
- [57] M. J. Trimpl, D. Boukerroui, E. P. Stride, K. A. Vallis, and M. J. Gooding, "Interactive contouring through contextual deep learning," *Medical Physics*, vol. 48, no. 6, pp. 2951–2959, 2021.
- [58] Y. Fang, D. Zhu, N. Zhou, L. Liu, and J. Yao, "Pipo-net: A semi-automatic and polygon-based annotation method for pathological images," in *2021 IEEE/RSJ International Conference on Intelligent Robots and Systems (IROS)*, pp. 2978–2984, IEEE, 2021.
- [59] M. Jahanifar, N. Z. Tajeddin, N. A. Koohbanani, and N. M. Rajpoot, "Robust interactive semantic segmentation of pathology images with minimal user input," in *Proceedings of the IEEE/CVF International Conference on Computer Vision*, pp. 674–683, 2021.
- [60] L. Sun, Z. Tian, Z. Chen, W. Luo, and S. Du, "An efficient interactive segmentation framework for medical images without pre-training," *Medical Physics*, 2022.
- [61] M. Shahedi, J. D. Dormer, M. Halicek, and B. Fei, "The effect of image annotation with minimal manual interaction for semiautomatic prostate segmentation in ct images using fully convolutional neural networks," *Medical physics*, vol. 49, no. 2, pp. 1153–1160, 2022.
- [62] A. Atzeni, L. Peter, E. Robinson, E. Blackburn, J. Althonayan, D. C. Alexander, and J. E. Iglesias, "Deep active learning for suggestive segmentation of biomedical image stacks via optimisation of dice scores and traced boundary length," *Medical Image Analysis*, vol. 81, p. 102549, 2022.
- [63] L. Bi, M. Fulham, and J. Kim, "Hyper-fusion network for semi-automatic segmentation of skin lesions," *Medical image analysis*, vol. 76, p. 102334, 2022.
- [64] Q. Liu, Z. Xu, Y. Jiao, and M. Niethammer, "isegformer: Interactive segmentation via transformers with application to 3d knee mr images," in *Medical Image Computing and Computer Assisted Intervention–MICCAI 2022: 25th International Conference, Singapore, September 18–22, 2022, Proceedings, Part V*, pp. 464–474, Springer, 2022.
- [65] M. Asad, L. Fidon, and T. Vercauteren, "Econet: Efficient convolutional online likelihood network for scribble-based interactive segmentation," in *International Conference on Medical Imaging with Deep Learning*, pp. 35–47, PMLR, 2022.
- [66] K. Gotkowski, C. Gonzalez, I. Kaltenborn, R. Fischbach, A. Bucher, and A. Mukhopadhyay, "i3deep: Efficient 3d interactive segmentation with the nnu-net," in *International Conference on Medical Imaging with Deep Learning*, pp. 441–456, PMLR, 2022.
- [67] A. Diaz-Pinto, P. Mehta, S. Alle, M. Asad, R. Brown, V. Nath, A. Ihsani, M. Antonelli, D. Palkovics, C. Pinter, *et al.*, "Deepedit: Deep editable learning for interactive segmentation of 3d medical images," in *Data Augmentation, Labelling, and Imperfections: Second MICCAI Workshop, DALI 2022, Held in Conjunction with MICCAI 2022, Singapore, September 22, 2022, Proceedings*, pp. 11–21, Springer, 2022.
- [68] W. Liu, C. Ma, Y. Yang, W. Xie, and Y. Zhang, "Transforming the interactive segmentation for medical imaging," in *Medical Image Computing and Computer Assisted Intervention–MICCAI 2022: 25th International Conference, Singapore, September 18–22, 2022, Proceedings, Part IV*, pp. 704–713, Springer, 2022.
- [69] L. Shi, X. Zhang, Y. Liu, and X. Han, "A hybrid propagation network for interactive volumetric image segmentation," in *Medical Image Computing and Computer Assisted Intervention–MICCAI 2022: 25th International Conference, Singapore, September 18–22, 2022, Proceedings, Part IV*, pp. 673–682, Springer, 2022.
- [70] M. Zhuang, Z. Chen, H. Wang, H. Tang, J. He, B. Qin, Y. Yang, X. Jin, M. Yu, B. Jin, *et al.*, "Anatomysketch: An extensible open-source software platform for medical image analysis algorithm development," *Journal of Digital Imaging*, pp. 1–11, 2022.
- [71] G. Galisot, J.-Y. Ramel, T. Brouard, E. Chaillou, and B. Serres, "Visual and structural feature combination in an interactive machine learning system for medical image segmentation," *Machine Learning with Applications*, vol. 8, p. 100294, 2022.
- [72] Z. Lin, Z. Zhang, L.-H. Han, and S.-P. Lu, "Multi-mode interactive image segmentation," in *Proceedings of the 30th ACM International Conference on Multimedia*, pp. 905–914, 2022.
- [73] R. Pirabakaran and N. Khan, "Interactive segmentation using u-net with weight map and dynamic user interactions," in *2022 44th Annual International Conference of the IEEE Engineering in Medicine & Biology Society (EMBC)*, pp. 4754–4757, IEEE, 2022.
- [74] I. Mikhailov, B. Chauveau, N. Bourdel, and A. Bartoli, "A deep learning-based interactive medical image segmentation framework," in *Applications of Medical Artificial Intelligence: First International Workshop, AMAI 2022, Held in Conjunction with MICCAI 2022, Singapore, September 18, 2022, Proceedings*, pp. 98–107, Springer, 2022.
- [75] R. Pirabakaran and N. Khan, "Improving interactive segmentation using a novel weighted loss function with an adaptive click size and two-stream fusion," in *2022 IEEE Eighth International Conference on Multimedia Big Data (BigMM)*, pp. 7–12, IEEE, 2022.
- [76] X. Chen, B. Zhou, L. Xiong, C. Zhao, L. Wang, Y. Zhang, and H. Xu, "Balancing regional and global information: An interactive segmentation framework for ultrasound breast lesion," *Biomedical Signal Processing and Control*, vol. 77, p. 103723, 2022.
- [77] S. Liang, H. Lu, M. Zang, X. Wang, Y. Jiao, T. Zhao, E. Y. Xu, and J. Xu, "Deep sed-net with interactive learning for multiple testicular cell types segmentation and cell composition analysis in mouse seminiferous tubules," *Cytometry Part A*, vol. 101, no. 8, pp. 658–674, 2022.
- [78] M. Ju, M. Lee, J. Lee, J. Yang, S. Yoon, and Y. Kim, "All you need is a few dots to label ct images for organ segmentation," *Applied Sciences*, vol. 12, no. 3, p. 1328, 2022.
- [79] W. Ma, S. Zheng, L. Zhang, H. Zhang, and Q. Dou, "Rapid model transfer for medical image segmentation via iterative human-in-the-loop update: from labelled public to unlabelled clinical datasets for multi-organ segmentation in ct," in *2022 IEEE 19th International Symposium on Biomedical Imaging (ISBI)*, pp. 1–5, IEEE, 2022.
- [80] T. Bai, A. Balagopal, M. Dohopolski, H. E. Morgan, R. McBeth, J. Tan, M.-H. Lin, D. J. Sher, D. Nguyen, and S. Jiang, "A proof-of-concept study of artificial intelligence-assisted contour editing," *Radiology: Artificial Intelligence*, vol. 4, no. 5, p. e210214, 2022.
- [81] T. Zhou, L. Li, G. Bredell, J. Li, J. Unkelbach, and E. Konukoglu, "Volumetric memory network for interactive medical image segmentation," *Medical Image Analysis*, vol. 83, p. 102599, 2023.

- [82] V. J. Hallitschke, T. Schlumberger, P. Kataliakos, Z. Marinov, M. Kim, L. Heiliger, C. Seibold, J. Kleesiek, and R. Stiefelwagen, "Multimodal interactive lung lesion segmentation: A framework for annotating pet/ct images based on physiological and anatomical cues," *arXiv preprint arXiv:2301.09914*, 2023.
- [83] Q. Liu, M. Zheng, B. Planche, Z. Gao, T. Chen, M. Niethammer, and Z. Wu, "Exploring cycle consistency learning in interactive volume segmentation," *arXiv preprint arXiv:2303.06493*, 2023.
- [84] A. Bruzadin, M. Boaventura, M. Colnago, R. G. Negri, and W. Casaca, "Learning label diffusion maps for semi-automatic segmentation of lung ct images with covid-19," *Neurocomputing*, vol. 522, pp. 24–38, 2023.
- [85] M. Asad, H. Williams, I. Mandal, S. Ather, J. Deprest, J. D'hooge, and T. Vercauteren, "Adaptive multi-scale online likelihood network for ai-assisted interactive segmentation," *arXiv preprint arXiv:2303.13696*, 2023.
- [86] A. H. Shahin, Y. Zhuang, and N. El-Zehiry, "From sparse to precise: A practical editing approach for intracardiac echocardiography segmentation," *arXiv preprint arXiv:2303.11041*, 2023.
- [87] M. Zhuang, Z. Chen, H. Wang, H. Tang, J. He, B. Qin, Y. Yang, X. Jin, M. Yu, B. Jin, *et al.*, "Efficient contour-based annotation by iterative deep learning for organ segmentation from volumetric medical images," *International Journal of Computer Assisted Radiology and Surgery*, vol. 18, no. 2, pp. 379–394, 2023.
- [88] D. J. Ho, M. H. Chui, C. M. Vanderbilt, J. Jung, M. E. Robson, C.-S. Park, J. Roh, and T. J. Fuchs, "Deep interactive learning-based ovarian cancer segmentation of h&e-stained whole slide images to study morphological patterns of brca mutation," *Journal of Pathology Informatics*, vol. 14, p. 100160, 2023.
- [89] Z. Wei, J. Ren, S. S. Korreman, and J. Nijkamp, "Towards interactive deep-learning for tumour segmentation in head and neck cancer radiotherapy," *Physics and Imaging in Radiation Oncology*, vol. 25, p. 100408, 2023.
- [90] M. Zhuang, Z. Chen, Y. Yang, L. Kettunen, and H. Wang, "Annotation-efficient training of medical image segmentation network based on scribble guidance in difficult areas," *International Journal of Computer Assisted Radiology and Surgery*, pp. 1–10, 2023.
- [91] Z. Marinov, R. Stiefelwagen, and J. Kleesiek, "Guiding the guidance: A comparative analysis of user guidance signals for interactive segmentation of volumetric images," *arXiv preprint arXiv:2303.06942*, 2023.
- [92] C. Qu, T. Zhang, H. Qiao, J. Liu, Y. Tang, A. Yuille, and Z. Zhou, "Abdomenatlas-8k: Annotating 8,000 ct volumes for multi-organ segmentation in three weeks," in *Thirty-seventh Conference on Neural Information Processing Systems Datasets and Benchmarks Track*, 2023.
- [93] M. A. Mazurowski, H. Dong, H. Gu, J. Yang, N. Konz, and Y. Zhang, "Segment anything model for medical image analysis: an experimental study," *arXiv preprint arXiv:2304.10517*, 2023.
- [94] R. Deng, C. Cui, Q. Liu, T. Yao, L. W. Remedios, S. Bao, B. A. Landman, L. E. Wheelless, L. A. Coburn, K. T. Wilson, *et al.*, "Segment anything model (sam) for digital pathology: Assess zero-shot segmentation on whole slide imaging," *arXiv preprint arXiv:2304.04155*, 2023.
- [95] S. Mohapatra, A. Gosai, and G. Schlaug, "Sam vs bet: A comparative study for brain extraction and segmentation of magnetic resonance images using deep learning," *arXiv preprint arXiv:2304.04738*, vol. 2, p. 4, 2023.
- [96] F. Putz, J. Grigo, T. Weissmann, P. Schubert, D. Hoefler, A. Goma, H. B. Tkhatay, A. Hagag, S. Lettmaier, B. Frey, *et al.*, "The segment anything foundation model achieves favorable brain tumor autosegmentation accuracy on mri to support radiotherapy treatment planning," *arXiv preprint arXiv:2304.07875*, 2023.
- [97] C. Hu and X. Li, "When sam meets medical images: An investigation of segment anything model (sam) on multi-phase liver tumor segmentation," *arXiv preprint arXiv:2304.08506*, 2023.
- [98] T. Chen, L. Zhu, C. Ding, R. Cao, S. Zhang, Y. Wang, Z. Li, L. Sun, P. Mao, and Y. Zang, "Sam fails to segment anything?—sam-adapter: Adapting sam in underperformed scenes: Camouflage, shadow, and more," *arXiv preprint arXiv:2304.09148*, 2023.
- [99] J. Wu, R. Fu, H. Fang, Y. Liu, Z. Wang, Y. Xu, Y. Jin, and T. Arbel, "Medical sam adapter: Adapting segment anything model for medical image segmentation," *arXiv preprint arXiv:2304.12620*, 2023.
- [100] Z. Qiu, Y. Hu, H. Li, and J. Liu, "Learnable ophthalmology sam," *arXiv preprint arXiv:2304.13425*, 2023.
- [101] S. He, R. Bao, J. Li, P. E. Grant, and Y. Ou, "Accuracy of segment-anything model (sam) in medical image segmentation tasks," *arXiv preprint arXiv:2304.09324*, 2023.
- [102] P. Shi, J. Qiu, S. M. D. Abaxi, H. Wei, F. P.-W. Lo, and W. Yuan, "Generalist vision foundation models for medical imaging: A case study of segment anything model on zero-shot medical segmentation," *Diagnostics*, vol. 13, no. 11, p. 1947, 2023.
- [103] B. Wang, A. Aboah, Z. Zhang, and U. Bagci, "Gazesam: What you see is what you segment," *arXiv preprint arXiv:2304.13844*, 2023.
- [104] M. Hu, Y. Li, and X. Yang, "Skinsam: Empowering skin cancer segmentation with segment anything model," *arXiv preprint arXiv:2304.13973*, 2023.
- [105] A. Wang, M. Islam, M. Xu, Y. Zhang, and H. Ren, "Sam meets robotic surgery: An empirical study in robustness perspective," *arXiv preprint arXiv:2304.14674*, 2023.
- [106] D. Cheng, Z. Qin, Z. Jiang, S. Zhang, Q. Lao, and K. Li, "Sam on medical images: A comprehensive study on three prompt modes," *arXiv preprint arXiv:2305.00035*, 2023.
- [107] C. Mattjie, L. V. de Moura, R. C. Ravazio, L. S. Kuppsinski, O. Parraga, M. M. Delucis, and R. C. Barros, "Exploring the zero-shot capabilities of the segment anything model (sam) in 2d medical imaging: A comprehensive evaluation and practical guideline," *arXiv preprint arXiv:2305.00109*, 2023.
- [108] Y. Li, M. Hu, and X. Yang, "Polyp-sam: Transfer sam for polyp segmentation," *arXiv preprint arXiv:2305.00293*, 2023.
- [109] J. Wu, "Promptnet: Toward interactive medical image segmentation," *arXiv preprint arXiv:2305.10300*, 2023.
- [110] M. Hu, Y. Li, and X. Yang, "Breastsam: A study of segment anything model for breast tumor detection in ultrasound images," *arXiv preprint arXiv:2305.12447*, 2023.
- [111] D. Lee, J. Park, S. Cook, s.-j. Yoo, D. Lee, and H. Choi, "Iamsam: Image-based analysis of molecular signatures using the segment-anything model," *bioRxiv*, pp. 2023–05, 2023.
- [112] Y. Gao, W. Xia, D. Hu, and X. Gao, "Desam: Decoupling segment anything model for generalizable medical image segmentation," *arXiv preprint arXiv:2306.00499*, 2023.
- [113] C. Shen, W. Li, Y. Zhang, and X. Wang, "Temporally-extended prompts optimization for sam in interactive medical image segmentation," *arXiv preprint arXiv:2306.08958*, 2023.
- [114] G. Ning, H. Liang, Z. Jiang, H. Zhang, and H. Liao, "The potential of 'segment anything'(sam) for universal intelligent ultrasound image guidance," *BioScience Trends*, 2023.
- [115] L. Zhang, Z. Liu, L. Zhang, Z. Wu, X. Yu, J. Holmes, H. Feng, H. Dai, X. Li, Q. Li, *et al.*, "Segment anything model (sam) for radiation oncology," *arXiv preprint arXiv:2306.11730*, 2023.
- [116] W. Lei, X. Wei, X. Zhang, K. Li, and S. Zhang, "Medlsam: Localize and segment anything model for 3d medical images," *arXiv preprint arXiv:2306.14752*, 2023.
- [117] G. Deng, K. Zou, K. Ren, M. Wang, X. Yuan, S. Ying, and H. Fu, "Sam-u: Multi-box prompts triggered uncertainty estimation for reliable sam in medical image," *arXiv preprint arXiv:2307.04973*, 2023.
- [118] S. Gong, Y. Zhong, W. Ma, J. Li, Z. Wang, J. Zhang, P.-A. Heng, and Q. Dou, "3dsam-adapter: Holistic adaptation of sam from 2d to 3d for promptable medical image segmentation," *arXiv preprint arXiv:2306.13465*, 2023.
- [119] Y. Huang, X. Yang, L. Liu, H. Zhou, A. Chang, X. Zhou, R. Chen, J. Yu, J. Chen, C. Chen, *et al.*, "Segment anything model for medical images?," *arXiv preprint arXiv:2304.14660*, 2023.
- [120] J. Ma and B. Wang, "Segment anything in medical images," *arXiv preprint arXiv:2304.12306*, 2023.
- [121] S. Roy, T. Wald, G. Koehler, M. R. Rokuss, N. Disch, J. Holzschuh, D. Zimmerer, and K. H. Maier-Hein, "Sam. md: Zero-shot medical image segmentation capabilities of the segment anything model," *arXiv preprint arXiv:2304.05396*, 2023.
- [122] H. Nickisch, C. Rother, P. Kohli, and C. Rhemann, "Learning an interactive segmentation system," in *Proceedings of the Seventh Indian Conference on Computer Vision, Graphics and Image Processing*, pp. 274–281, 2010.
- [123] J. Canny, "A computational approach to edge detection," *IEEE Transactions on pattern analysis and machine intelligence*, no. 6, pp. 679–698, 1986.
- [124] W. Pedrycz, "Shadowed sets: representing and processing fuzzy sets," *IEEE Transactions on Systems, Man, and Cybernetics, Part B (Cybernetics)*, vol. 28, no. 1, pp. 103–109, 1998.
- [125] D. Barbosa, T. Diertenbeck, J. Schaerer, J. D'hooge, D. Friboulet, and O. Bernard, "B-spline explicit active surfaces: an efficient framework for real-time 3-d region-based segmentation," *IEEE transactions on image processing*, vol. 21, no. 1, pp. 241–251, 2011.
- [126] A. Yezzi Jr, A. Tsai, and A. Willsky, "A fully global approach to image segmentation via coupled curve evolution equations," *Journal of Visual Communication and Image Representation*, vol. 13, no. 1-2, pp. 195–216, 2002.

- [127] O. Ronneberger, P. Fischer, and T. Brox, "U-net: Convolutional networks for biomedical image segmentation," in *Medical Image Computing and Computer-Assisted Intervention—MICCAI 2015: 18th International Conference, Munich, Germany, October 5-9, 2015, Proceedings, Part III* 18, pp. 234–241, Springer, 2015.
- [128] S. Hochreiter and J. Schmidhuber, "Long short-term memory," *Neural computation*, vol. 9, no. 8, pp. 1735–1780, 1997.
- [129] Z.-H. Zhou, "A brief introduction to weakly supervised learning," *National science review*, vol. 5, no. 1, pp. 44–53, 2018.
- [130] J. Hu, L. Shen, and G. Sun, "Squeeze-and-excitation networks," in *Proceedings of the IEEE conference on computer vision and pattern recognition*, pp. 7132–7141, 2018.
- [131] Y. Y. Boykov and M.-P. Jolly, "Interactive graph cuts for optimal boundary & region segmentation of objects in nd images," in *Proceedings eighth IEEE international conference on computer vision. ICCV 2001*, vol. 1, pp. 105–112, IEEE, 2001.
- [132] P. Salembier and L. Garrido, "Binary partition tree as an efficient representation for image processing, segmentation, and information retrieval," *IEEE transactions on Image Processing*, vol. 9, no. 4, pp. 561–576, 2000.
- [133] R. Achanta, A. Shaji, K. Smith, A. Lucchi, P. Fua, and S. Süsstrunk, "Slic superpixels compared to state-of-the-art superpixel methods," *IEEE transactions on pattern analysis and machine intelligence*, vol. 34, no. 11, pp. 2274–2282, 2012.
- [134] M. Jenkinson, M. Pechaud, S. Smith, *et al.*, "Bet2: Mr-based estimation of brain, skull and scalp surfaces," in *Eleventh annual meeting of the organization for human brain mapping*, vol. 17, p. 167, Toronto., 2005.
- [135] A. Hatamizadeh, V. Nath, Y. Tang, D. Yang, H. R. Roth, and D. Xu, "Swin unetr: Swin transformers for semantic segmentation of brain tumors in mri images," in *International MICCAI Brainlesion Workshop*, pp. 272–284, Springer, 2021.
- [136] F. Isensee, P. F. Jaeger, S. A. Kohl, J. Petersen, and K. H. Maier-Hein, "nnu-net: a self-configuring method for deep learning-based biomedical image segmentation," *Nature methods*, vol. 18, no. 2, pp. 203–211, 2021.
- [137] A. Kirillov, E. Mintun, N. Ravi, H. Mao, C. Rolland, L. Gustafson, T. Xiao, S. Whitehead, A. C. Berg, W.-Y. Lo, *et al.*, "Segment anything," *arXiv preprint arXiv:2304.02643*, 2023.
- [138] A. Dosovitskiy, L. Beyer, A. Kolesnikov, D. Weissenborn, X. Zhai, T. Unterthiner, M. Dehghani, M. Minderer, G. Heigold, S. Gelly, *et al.*, "An image is worth 16x16 words: Transformers for image recognition at scale," *arXiv preprint arXiv:2010.11929*, 2020.
- [139] D. Moher, A. Liberati, J. Tetzlaff, D. G. Altman, and P. Group*, "Preferred reporting items for systematic reviews and meta-analyses: the prisma statement," *Annals of internal medicine*, vol. 151, no. 4, pp. 264–269, 2009.
- [140] N. Xu, B. Price, S. Cohen, J. Yang, and T. S. Huang, "Deep interactive object selection," in *Proceedings of the IEEE conference on computer vision and pattern recognition*, pp. 373–381, 2016.
- [141] C. Rother, V. Kolmogorov, and A. Blake, "grabcut" interactive foreground extraction using iterated graph cuts," *ACM transactions on graphics (TOG)*, vol. 23, no. 3, pp. 309–314, 2004.
- [142] F. Perazzi, J. Pont-Tuset, B. McWilliams, L. Van Gool, M. Gross, and A. Sorkine-Hornung, "A benchmark dataset and evaluation methodology for video object segmentation," in *Proceedings of the IEEE conference on computer vision and pattern recognition*, pp. 724–732, 2016.
- [143] M. Everingham, L. Van Gool, C. K. Williams, J. Winn, and A. Zisserman, "The pascal visual object classes (voc) challenge," *International journal of computer vision*, vol. 88, pp. 303–338, 2010.
- [144] B. Hariharan, P. Arbeláez, L. Bourdev, S. Maji, and J. Malik, "Semantic contours from inverse detectors," in *2011 international conference on computer vision*, pp. 991–998, IEEE, 2011.
- [145] K. McGuinness and N. E. O'connor, "A comparative evaluation of interactive segmentation algorithms," *Pattern Recognition*, vol. 43, no. 2, pp. 434–444, 2010.
- [146] M. Eisenmann, A. Reinke, V. Weru, M. D. Tizabi, F. Isensee, T. J. Adler, S. Ali, V. Andrearczyk, M. Aubreville, U. Baid, *et al.*, "Why is the winner the best?," in *Proceedings of the IEEE/CVF Conference on Computer Vision and Pattern Recognition*, pp. 19955–19966, 2023.
- [147] S. G. Hart and L. E. Staveland, "Development of nasa-tlx (task load index): Results of empirical and theoretical research," in *Advances in psychology*, vol. 52, pp. 139–183, Elsevier, 1988.
- [148] J. Brooke, "Sus: a "quick and dirty" usability," *Usability evaluation in industry*, vol. 189, no. 3, pp. 189–194, 1996.
- [149] A. Diaz-Pinto, S. Alle, V. Nath, Y. Tang, A. Ihsani, M. Asad, F. Pérez-García, P. Mehta, W. Li, M. Flores, *et al.*, "Monai label: A framework for ai-assisted interactive labeling of 3d medical images," *arXiv preprint arXiv:2203.12362*, 2022.
- [150] K. A. Philbrick, A. D. Weston, Z. Akkus, T. L. Kline, P. Korfiatis, T. Sakinis, P. Kostandy, A. Boonrod, A. Zeinoddini, N. Takahashi, *et al.*, "Ril-contour: a medical imaging dataset annotation tool for and with deep learning," *Journal of digital imaging*, vol. 32, pp. 571–581, 2019.
- [151] P. D. Lösel, T. van de Kamp, A. Jayme, A. Ershov, T. Faragó, O. Pichler, N. Tan Jerome, N. Aadeputu, S. Bremer, S. A. Chilingaryan, *et al.*, "Introducing biomedisa as an open-source online platform for biomedical image segmentation," *Nature communications*, vol. 11, no. 1, p. 5577, 2020.
- [152] S. Mahadevan, P. Voigtlaender, and B. Leibe, "Iteratively trained interactive segmentation," in *British Machine Vision Conference (BMVC)*, 2018.
- [153] M. Kass, A. Witkin, and D. Terzopoulos, "Snakes: Active contour models," *International journal of computer vision*, vol. 1, no. 4, pp. 321–331, 1988.
- [154] S. Gatidis, M. Früh, M. Fabritius, S. Gu, K. Nikolaou, C. La Fougère, J. Ye, J. He, Y. Peng, L. Bi, *et al.*, "The autopen challenge: Towards fully automated lesion segmentation in oncologic pet/ct imaging," 2023.
- [155] F. Zhao and X. Xie, "An overview of interactive medical image segmentation," *Annals of the BMVA*, vol. 2013, no. 7, pp. 1–22, 2013.
- [156] S. D. Olabarriga and A. W. Smeulders, "Interaction in the segmentation of medical images: A survey," *Medical image analysis*, vol. 5, no. 2, pp. 127–142, 2001.
- [157] H. Ramadan, C. Lachqar, and H. Tairi, "A survey of recent interactive image segmentation methods," *Computational visual media*, vol. 36, pp. 355–384, 2020.
- [158] Ç. Kaymak and A. Uçar, "A brief survey and an application of semantic image segmentation for autonomous driving," *Handbook of Deep Learning Applications*, pp. 161–200, 2019.
- [159] D. Tabernik, S. Šela, J. Skvarč, and D. Škočaj, "Segmentation-based deep-learning approach for surface-defect detection," *Journal of Intelligent Manufacturing*, vol. 31, no. 3, pp. 759–776, 2020.
- [160] G. Litjens, T. Kooi, B. E. Bejnordi, A. A. A. Setio, F. Ciompi, M. Ghafoorian, J. A. Van Der Laak, B. Van Ginneken, and C. I. Sánchez, "A survey on deep learning in medical image analysis," *Medical image analysis*, vol. 42, pp. 60–88, 2017.
- [161] M. Bakator and D. Radosav, "Deep learning and medical diagnosis: A review of literature," *Multimodal Technologies and Interaction*, vol. 2, no. 3, p. 47, 2018.
- [162] B. H. Menze, A. Jakab, S. Bauer, J. Kalpathy-Cramer, K. Farahani, J. Kirby, Y. Burren, N. Porz, J. Slotboom, R. Wiest, *et al.*, "The multimodal brain tumor image segmentation benchmark (brats)," *IEEE transactions on medical imaging*, vol. 34, no. 10, pp. 1993–2024, 2014.
- [163] M. Antonelli, A. Reinke, S. Bakas, K. Farahani, A. Kopp-Schneider, B. A. Landman, G. Litjens, B. Menze, O. Ronneberger, R. M. Summers, *et al.*, "The medical segmentation decathlon," *Nature communications*, vol. 13, no. 1, p. 4128, 2022.
- [164] P. Bilic, P. Christ, H. B. Li, E. Vorontsov, A. Ben-Cohen, G. Kaissis, A. Szeskin, C. Jacobs, G. E. H. Mamani, G. Chartrand, *et al.*, "The liver tumor segmentation benchmark (lits)," *Medical Image Analysis*, vol. 84, p. 102680, 2023.
- [165] L. Maier-Hein, B. Menze, *et al.*, "Metrics reloaded: Pitfalls and recommendations for image analysis validation," *arXiv.org*, no. 2206.01653, 2022.
- [166] P. Krähnbehül and V. Koltun, "Efficient inference in fully connected crfs with gaussian edge potentials," *Advances in neural information processing systems*, vol. 24, 2011.
- [167] A. E. Lefohn, J. E. Cates, and R. T. Whitaker, "Interactive, gpu-based level sets for 3d segmentation," in *Medical Image Computing and Computer-Assisted Intervention—MICCAI 2003: 6th International Conference, Montréal, Canada, November 15-18, 2003. Proceedings 6*, pp. 564–572, Springer, 2003.
- [168] C. Sommer, C. Strahle, U. Koethe, and F. A. Hamprecht, "Ilastik: Interactive learning and segmentation toolkit," in *2011 IEEE international symposium on biomedical imaging: From nano to macro*, pp. 230–233, IEEE, 2011.
- [169] P. A. Yushkevich, Y. Gao, and G. Gerig, "Itk-snap: An interactive tool for semi-automatic segmentation of multi-modality biomedical images," in *2016 38th annual international conference of the IEEE engineering in medicine and biology society (EMBC)*, pp. 3342–3345, IEEE, 2016.

- [170] A. Reinke, M. D. Tizabi, M. Baumgartner, M. Eisenmann, D. Heckmann-Nötzel, A. E. Kavur, T. Rädtsch, C. H. Sudre, L. Acion, M. Antonelli, *et al.*, “Understanding metric-related pitfalls in image analysis validation,” *ArXiv*, 2023.
- [171] S. Nikolov, S. Blackwell, A. Zverovitch, R. Mendes, M. Livne, J. De Fauw, Y. Patel, C. Meyer, H. Askham, B. Romera-Paredes, *et al.*, “Clinically applicable segmentation of head and neck anatomy for radiotherapy: deep learning algorithm development and validation study,” *Journal of medical Internet research*, vol. 23, no. 7, p. e26151, 2021.
- [172] R. Li and X. Chen, “An efficient interactive multi-label segmentation tool for 2d and 3d medical images using fully connected conditional random field,” *Computer Methods and Programs in Biomedicine*, vol. 213, p. 106534, 2022.
- [173] I. Wolf, M. Vetter, I. Wegner, T. Böttger, M. Nolden, M. Schöbinger, M. Hastenteufel, T. Kunert, and H.-P. Meinzer, “The medical imaging interaction toolkit,” *Medical image analysis*, vol. 9, no. 6, pp. 594–604, 2005.
- [174] G. Wang, X. Luo, R. Gu, S. Yang, Y. Qu, S. Zhai, Q. Zhao, K. Li, and S. Zhang, “Pymic: A deep learning toolkit for annotation-efficient medical image segmentation,” *Computer Methods and Programs in Biomedicine*, vol. 231, p. 107398, 2023.
- [175] L. Castrejon, K. Kundu, R. Urtasun, and S. Fidler, “Annotating object instances with a polygon-rnn,” in *Proceedings of the IEEE conference on computer vision and pattern recognition*, pp. 5230–5238, 2017.
- [176] K.-K. Maninis, S. Caelles, J. Pont-Tuset, and L. Van Gool, “Deep extreme cut: From extreme points to object segmentation,” in *Proceedings of the IEEE conference on computer vision and pattern recognition*, pp. 616–625, 2018.
- [177] K. Sofiiuk, I. Petrov, O. Barinova, and A. Konushin, “f-brs: Rethinking backpropagating refinement for interactive segmentation,” in *Proceedings of the IEEE/CVF Conference on Computer Vision and Pattern Recognition*, pp. 8623–8632, 2020.
- [178] W.-D. Jang and C.-S. Kim, “Interactive image segmentation via back-propagating refinement scheme,” in *Proceedings of the IEEE/CVF Conference on Computer Vision and Pattern Recognition*, pp. 5297–5306, 2019.
- [179] Z. Li, Q. Chen, and V. Koltun, “Interactive image segmentation with latent diversity,” in *Proceedings of the IEEE Conference on Computer Vision and Pattern Recognition*, pp. 577–585, 2018.
- [180] A. S. A. Khaizi, R. A. M. Rosidi, H.-S. Gan, and K. A. Sayuti, “A mini review on the design of interactive tool for medical image segmentation,” in *2017 International Conference on Engineering Technology and Technopreneurship (ICE2T)*, pp. 1–5, 2017.
- [181] A. Criminisi, T. Sharp, and A. Blake, “Geos: Geodesic image segmentation,” in *Computer Vision—ECCV 2008: 10th European Conference on Computer Vision, Marseille, France, October 12–18, 2008, Proceedings, Part I 10*, pp. 99–112, Springer, 2008.
- [182] P. J. Toivanen, “New geodesic distance transforms for gray-scale images,” *Pattern Recognition Letters*, vol. 17, no. 5, pp. 437–450, 1996.
- [183] L. Grady, “Random walks for image segmentation,” *IEEE transactions on pattern analysis and machine intelligence*, vol. 28, no. 11, pp. 1768–1783, 2006.
- [184] S. Peleg and A. Rosenfeld, “A min-max medial axis transformation,” *IEEE Transactions on Pattern Analysis and Machine Intelligence*, no. 2, pp. 208–210, 1981.